IOP Publishing Quantum Sci. Technol. 8 (2023) 015015 https://doi.org/10.1088/2058-9565/aca4ee

Quantum Science and Technology

OPEN ACCESS

RECEIVED
28 July 2022

REVISED
17 November 2022

ACCEPTED FOR PUBLICATION
22 November 2022

PUBLISHED
5 December 2022

PAPER

Quantum correlations in molecules: from quantum resourcing to chemical bonding

Lexin Ding[1,2], **Stefan Knecht**[3,4,*], **Zoltán Zimborás**[3,5,6] **and Christian Schilling**[1,2,*]

[1] Faculty of Physics, Arnold Sommerfeld Centre for Theoretical Physics (ASC), Ludwig-Maximilians-Universität München, Theresienstr. 37, 80333 München, Germany
[2] Munich Center for Quantum Science and Technology (MCQST), Schellingstrasse 4, 80799 München, Germany
[3] Algorithmiq Ltd, Kanavakatu 3C, FI-00160 Helsinki, Finland
[4] ETH Zürich, Laboratory for Physical Chemistry, Vladimir-Prelog-Weg 2, 8093 Zürich, Switzerland
[5] Theoretical Physics Department, Wigner Research Centre for Physics, PO Box 49, H-1525 Budapest, Hungary
[6] Eötvös Lorán University, Pázmány Péter sétány. 1/C, 1117 Budapest, Hungary
[*] Authors to whom any correspondence should be addressed.

E-mail: stefan@algorithmiq.fi and c.schilling@physik.uni-muenchen.de

Keywords: quantum correlations, entanglement, molecular systems, chemical bond, fermions, quantum resources

Abstract

The second quantum revolution is all about exploiting the quantum nature of atoms and molecules to execute quantum information processing tasks. To boost this growing endeavor and by anticipating the key role of quantum chemistry therein, our work establishes a framework for systematically exploring, quantifying and dissecting correlation effects in molecules. By utilizing the geometric picture of quantum states we compare—on a unified basis and in an operationally meaningful way—total, quantum and classical correlation and entanglement in molecular ground states. To unlock and maximize the quantum informational resourcefulness of molecules an orbital optimization scheme is developed, leading to a paradigm-shifting insight: a single covalent bond equates to the entanglement $2\ln(2)$. This novel and more versatile perspective on electronic structure suggests a generalization of valence bond theory, overcoming deficiencies of modern chemical bonding theories.

1. Introduction

In light of the fast-approaching second quantum revolution [1–3], soon we will be able to comprehensively exploit the quantum nature of chemical systems to our advantage. This historic opportunity has boosted many studies on fermionic correlation and entanglement in the quantum information (QI) community [4–17], with an emphasis on the conceptual formalism and resource utilization aspects. Independently, fermionic correlation has been used in the quantum chemistry (QC) community to describe the electronic structure of chemical systems [18–29] and to improve as well as optimize the initial ansatz of numerical methods [30–32]. Yet, only rudimentary QI tools have thus far been widely adopted for such type of studies. It is therefore the ultimate motivation of our work to propel the on-going second quantum revolution by combining the expertise of both the QI and QC community and to harness synergies. To achieve this, three important facets need to be furnished. Firstly, the dissection of classical and quantum correlation effects still needs to be distinctly and visibly advocated, evidenced by the fact that only the von Neumann entropy has been so far systematically applied. Secondly, this simple quantity is even erroneously calculated, by ignoring important fermionic superselection rules [33, 34] (SSR). Violation of these rules, in the context of the second quantum revolution, leads to a gross overestimation of the accessible quantum resource. Thirdly, the subject of correlation analysis has been primarily limited to the canonical, delocalized orbitals. Accordingly, these three points urge us to provide in the present work tailored tools for operationally meaningful quantification and categorization of the correlation in chemical system.

To this end, we turn to the plethora of correlation quantities offered by the QI community, although their application to chemical systems is not without hurdles. Relevant chemical concepts and interesting

phenomena are often concerned with a particular subregion of molecular systems. For instance, the concept of a chemical bond often refers to just two neighboring atoms. Yet, their quantum state is not pure anymore due to their interaction with the other atoms in the molecule. Accordingly, the easy-to-calculate von Neumann entropy is not a valid measure of correlation or entanglement anymore. Moreover, various definitions of quantum correlation, classical correlation [35–37] and entanglement [38–40] for mixed states from QI have often different conceptual origins. The unpleasant consequence is that one cannot compare the respective values against each other, just as it does not make sense in chemistry to compare molecular energy values referring to different systems of physical units. Hence, it is one of our main goals to offer an appealing geometric picture of quantum states in which all these correlation quantities can be defined on the same footing.

With a suitable QI framework at hand we can then address the following fundamental question: What is the QI resource content of a molecule in general and of a chemical bond in particular? Based on an orbital optimization scheme, we identify fully localized orbitals as the adequate reference basis for realizing and extracting this total entanglement. Due to the connection between electronic structure and entanglement, this key observation of our work will also bridge the two pillars of chemical bonding theories: molecular orbital [41, 42] (MO) theory and valence bond [43, 44] (VB) theory. In MO theory, a bond of order one is represented by a fully occupied bonding MO (and its empty antibonding partner). By contrast, VB theory describes a bond with a pair of coupled atomic orbitals, thus offering an attractive local perspective of bonding. Adversely, VB theory by itself does not reach modern chemical accuracy, and a quantitative measure for the correlation between the atomic orbitals is lacking. Our work fuses these two distinctively different pictures, and makes use of the correlation between atomic-like MOs to unveil the unique orbital pairing structures in chemical bonds: A single covalent bond is equivalent to the orbital entanglement content $2\ln(2)$. This value exceeds by an order of magnitude the numbers reported in previous studies [19–28]. This in turn emphasizes that QI tools applied to delocalized orbitals describe primarily the validity of the independent electron-pair picture rather than the bonding structure of molecular systems.

The paper is structured as follows. We start with a brief overview of fermionic correlation in section 2 for the less experienced audience, and for later use. Then in section 3 we illustrate these concepts with two analytic examples, and explore the relation between orbital entanglement and bonding. Finally in sections 4 and 5 we demonstrate in realistic molecular systems the effect of orbital localization on maximizing their quantum resource, as well as revealing their bonding structures.

2. Concepts

In this section we will give a brief overview of fermionic correlation and entanglement. Specifically, we will explain (a) how are various correlation quantities such as entanglement and quantum correlation quantified in QI, and (b) how can one transfer these QI concepts, which are formulated for distinguishable systems, to indistinguishable fermions. Both aspects are not only crucial for understanding the main results of this work, but also potentially beneficial for specialists from QI or QC communities who would like to also work on this interdisciplinary topic. Experts on fermionic entanglement shall feel free to skip this section and return in case any unfamiliar concepts may appear in the proceeding sections.

2.1. Geometry of quantum states

In order to set the stage for what follows, it will be essential to first recall and discuss basic geometric aspects of the space of quantum states. It is exactly this geometric picture which will namely allow us to quantify and compare on a unified basis total, quantum and classical correlation and entanglement in molecular quantum systems.

Let us start by considering a complex finite-dimensional Hilbert space $\mathcal{H}$ of dimension d and denote the algebra of linear operators acting on $\mathcal{H}$ by $\mathcal{B}(\mathcal{H})$. The corresponding set $\mathcal{D}$ of density operators is given by all Hermitian operators ρ on $\mathcal{H}$ which are positive-semidefinite $\rho \geqslant 0$ (i.e. ρ has non-negative eigenvalues), and trace-normalized to unity,

$$\mathcal{D} = \{\rho \in \mathcal{B}(\mathcal{H}) \,|\, \rho^\dagger = \rho,\, \rho \geqslant 0,\, \mathrm{Tr}[\rho] = 1\}\,. \tag{1}$$

As it is illustrated in figure 1, the set $\mathcal{D}$ is convex since the convex combination $p\rho + (1-p)\tilde{\rho}$ of any two density operators $\rho, \tilde{\rho} \in \mathcal{D}$ and any $0 \leqslant p \leqslant 1$ is again a density operator. In order to develop a better intuition for $\mathcal{D}$, we observe that a density operator ρ lies on the boundary of $\mathcal{D}$ if it is not strictly positive, that is, at least one of its eigenvalues vanishes. A particularly important subset of boundary points is given by the extremal points of $\mathcal{D}$. These are per definition those 'points' $\rho \in \mathcal{D}$ which cannot be written as convex

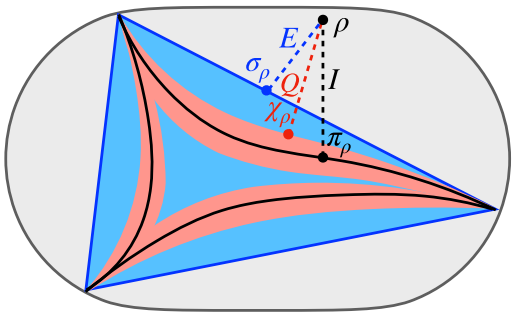

Figure 1. Schematic illustration of the state space $\mathcal{D}$. The subsets of uncorrelated ($\mathcal{D}_0$), classically correlated ($\mathcal{D}_{\rm cl}$) and separable states ($\mathcal{D}_{\rm sep}$) are shown in black, red and blue, respectively. The corresponding measures of total correlation I, quantum correlation Q and entanglement E are given by the quantum relative entropy (4) of ρ minimized with respect to those sets, with corresponding minimizers π_ρ, χ_ρ and σ_ρ.

combinations of other points in $\mathcal{D}$. One easily verifies that a density operator ρ is extremal if and only if it is a pure state

$$\rho \equiv |\Psi\rangle\langle\Psi| \quad \text{with } |\Psi\rangle \in \mathcal{H}\,, \tag{2}$$

or, equivalently, if ρ has eigenvalues $\{1, 0, \ldots, 0\}$.

Since the space $\mathcal{D}$ of density operators is a subset of the Euclidean vector space of linear operators on $\mathcal{H}$ (or equivalently just $\mathbb{C}^{d\times d}$) we can introduce a notion of distances and angles in a straightforward manner. To this end, we introduce the Hilbert–Schmidt inner product on $\mathcal{B}(\mathcal{H})$,

$$\langle \hat{A}, \hat{B}\rangle \equiv \mathrm{Tr}[\hat{A}^\dagger \hat{B}] \tag{3}$$

where $\hat{A}, \hat{B} \in \mathcal{B}(\mathcal{H})$ are linear operators. By employing either the induced norm, any other metric or a generalized distance function we can then quantify the similarity of quantum states. The huge advantage of this approach lies in the universality of its predictions: Whenever two density operators are close to each other, the same follows as a mathematical consequence for their expectation values for *any* choice of observable. A prominent generalized distance function [45] is given by the quantum relative entropy [38, 46]

$$S(\rho||\sigma) \equiv \mathrm{Tr}[\rho(\ln\rho - \ln\sigma)]\,. \tag{4}$$

Its relevance for quantum sciences in general and our work in particular originates from its distinctive information-theoretical meaning. It describes by concise means '*how difficult it is to distinguish the state ρ from the state σ*' [47] (see also [48]).

2.2. Overview of various correlation types

The QI theoretical concepts of correlation and entanglement refer to a notion of subsystems [40, 49, 50]. In order to discuss them in the context of *bipartite* systems, we assume that our total system comprises two *distinguishable* subsystems A and B. The corresponding Hilbert space then takes the form

$$\mathcal{H} = \mathcal{H}_A \otimes \mathcal{H}_B \tag{5}$$

and likewise for the algebra of observables,

$$\mathcal{B}(\mathcal{H}) = \mathcal{B}(\mathcal{H}_A) \otimes \mathcal{B}(\mathcal{H}_B)\,. \tag{6}$$

To motivate the concept of total correlation let us consider two local measurements, with corresponding observables $\hat{A} \in \mathcal{B}(\mathcal{H}_A)$ of subsystem A and $\hat{B} \in \mathcal{B}(\mathcal{H}_B)$ of subsystem B. The correlation between these two measurements is described by the correlation function

$$\begin{aligned}\mathcal{C}(\hat{A}, \hat{B}) &\equiv \langle \hat{A}\otimes\hat{B}\rangle_\rho - \langle \hat{A}\otimes\hat{1}_B\rangle_\rho \langle \hat{1}_A\otimes\hat{B}\rangle_\rho \\ &\equiv \langle \hat{A}\otimes\hat{B}\rangle_\rho - \langle \hat{A}\rangle_{\rho_A}\langle \hat{B}\rangle_{\rho_B}\,,\end{aligned} \tag{7}$$

where $\rho_{A/B} \equiv \mathrm{Tr}_{B/A}[\rho_{AB}]$ denotes the reduced density operator of ρ for subsystem A/B and $\hat{1}_{A/B}$ the identity operator on $\mathcal{H}_{A/B}$. The crucial observation is now that a vanishing correlation function, $\mathcal{C}(\hat{A}, \hat{B}) = 0$, does

not necessarily imply the same for any other pair of local observables $\hat{A}', \hat{B}'$. This in turn strongly suggests the notion of uncorrelated states: A density operator ρ is called uncorrelated if and only if its correlation function (7) vanishes for *all* pairs of local observables $\hat{A}, \hat{B}$. As long as the algebra $\mathcal{A}_{A/B}$ of physical observables of system A/B includes all linear operators on $\mathcal{H}_{A/B}$, this is equivalent to the factorization of ρ into its reduced states, $\rho = \rho_A \otimes \rho_B$. The corresponding set

$$\mathcal{D}_0 \equiv \{\rho = \rho_A \otimes \rho_B\} \tag{8}$$

of all uncorrelated states is schematically illustrated in figure 1. By referring to this geometric picture, a straightforward definition of the *total* correlation $I(\rho)$ contained in a quantum state ρ follows. It is given as the minimal 'distance' of ρ to the set $\mathcal{D}_0$,

$$\begin{aligned} I(\rho) &\equiv \min_{\pi \in \mathcal{D}_0} S(\rho||\pi) \\ &= S(\rho_A) + S(\rho_B) - S(\rho)\,, \end{aligned} \tag{9}$$

measured in terms of the quantum relative entropy $S(\cdot||\cdot)$, where $S(\rho) \equiv -\mathrm{Tr}[\rho \ln \rho]$ denotes the von Neumann entropy. Remarkably, the minimization in (9) can be executed analytically, leading to the mutual information (second line) where the closest uncorrelated state follows as $\pi_\rho = \rho_A \otimes \rho_B$ [51]. Coming back to our motivation, we present an important relation between the total correlation and correlation functions which follows directly from results presented in [52, 53] (see [54] for a detailed derivation),

$$\frac{|\mathcal{C}(\hat{A}, \hat{B})|}{\|\hat{A}\|_{\mathrm{op}}\, \|\hat{B}\|_{\mathrm{op}}} \leqslant \sqrt{2}\, \sqrt{I(\rho)}\,. \tag{10}$$

Here, $\|\hat{A}\|_{\mathrm{op}}$ denotes the operator norm of $\hat{A}$, i.e. the largest absolute value of its eigenvalues. Relation (10) confirms in quantitative terms that whenever a quantum state is close to the set $\mathcal{D}_0$ of uncorrelated states then its correlation function is small for *any* choice of local observables $\hat{A}, \hat{B}$. This highlights again the strength of QI theoretical concepts which is based on the universal character of their predictions.

Due to the information theoretical meaning of the quantum relative entropy (4), the total correlation (9) quantifies the additional information content in the state ρ beyond the information content in $\rho_A \otimes \rho_B$ (local information). The term 'total' emphasizes here that $I(\rho)$ includes both classical and quantum correlations. In order to explore and conclusively understand the significance of either correlation part in chemical bonding and QC in general, concise definitions of quantum correlation and classical correlations are needed as well. We first start, however, with the most prominent type of quantum correlation, the entanglement.

Separable or unentangled states are precisely those states that can be prepared by distant laboratories using local operations and classical communication only [49]. With local operations, two distant parties can prepare any uncorrelated state $\rho_A \otimes \rho_B$. In combination with classical communication arbitrary mixtures of uncorrelated states can be realized. Hence, the convex set of separable states is given by

$$\mathcal{D}_{\mathrm{sep}} \equiv \left\{ \sigma = \sum_i p_i \sigma_A^{(i)} \otimes \sigma_B^{(i)}, p_i > 0, \sum_i p_i = 1 \right\}. \tag{11}$$

As it is illustrated in figure 1, this set is indeed nothing else than the convex hull of $\mathcal{D}_0$. Any state ρ that is not separable is called entangled. In complete analogy to the quantification of total correlation, the entanglement in ρ is quantified through the geometric picture [55]

$$E(\rho) \equiv \min_{\sigma \in \mathcal{D}_{\mathrm{sep}}} S(\rho||\sigma) = S(\rho||\sigma_\rho)\,. \tag{12}$$

For general mixed states, no closed expression exists for this *relative entropy of entanglement*, except for highly symmetric states [56]. This unpleasant fact is due to the involved structure of the set (11) of separable states and the resulting complexity of its boundary. For pure states $\rho \equiv |\Psi\rangle\langle\Psi|$, however, (12) simplifies to a closed expression [38]

$$E(|\Psi\rangle\langle\Psi|) = S(\rho_A) = S(\rho_B). \tag{13}$$

As a consistency check, we recall that the spectra of the reduced states ρ_A and ρ_B are indeed identical, as it is guaranteed by the Schmidt decomposition [57] of $|\Psi\rangle$.

Entanglement is certainly a key concept of quantum physics [58–60] and its broad significance as a resource for realizing QI processing tasks is undeniable [61–64]. Yet, there also exist quantum correlations *beyond* entanglement. In order to explain this crucial aspect of our work, and in analogy to the definition of total correlation and entanglement, we first characterize the family of states with zero quantum correlation [51, 65, 66] (illustrated as pink region in figure 1):

$$\mathcal{D}_{\mathrm{cl}} \equiv \left\{ \chi = \sum_{i,j} p_{ij} |i\rangle\langle i| \otimes |j\rangle\langle j| \right\}. \tag{14}$$

On the right-hand side, $\{|i\rangle\}$ and $\{|j\rangle\}$ could be *any* sets of orthonormal states in the Hilbert spaces of subsystems A and B, respectively and $p_{ij} > 0$, $\sum_{ij} p_{ij} = 1$. The states in (14) are indeed *classical* in the following sense. There exists joint local measurement $\{P_A^{(i)} \otimes P_B^{(j)}\}$ which leave the state ρ unchanged, namely those with $\{P_{A/B}^{(i)}\}$ projecting onto the local eigenstates $\{|i\rangle\}$ and $\{|j\rangle\}$ of ρ. Therefore the correlation encoded in the resulting joint probability distribution $\{p_{ij}\}$ has to be purely classical [66]. Any state not in $\mathcal{D}_{\mathrm{cl}}$ then contains quantum correlation.

By referring again to the geometric picture of quantum states, the quantum correlation in ρ is quantified as its minimized quantum relative entropy with respect to the set of classically correlated states [51] (with the minimizer denoted by χ_ρ).

$$Q(\rho) \equiv \min_{\chi \in \mathcal{D}_{\mathrm{cl}}} S(\rho||\chi) \equiv S(\rho||\chi_\rho). \tag{15}$$

Note that $\mathcal{D}_0 \subseteq \mathcal{D}_{\mathrm{cl}}$ since every uncorrelated state $\rho_A \otimes \rho_B \equiv \left(\sum_i p_A^{(i)} |i\rangle\langle i|\right) \otimes \left(\sum_j p_B^{(j)} |j\rangle\langle j|\right)$ can be written as in (14), namely with $p_{ij} = p_A^{(i)} p_B^{(j)}$. On the other hand, the set $\mathcal{D}_{\mathrm{sep}}$ in (11) is strictly larger than $\mathcal{D}_{\mathrm{cl}}$. This is due to the fact that in the former $\{\sigma_{A/B}^i\}$ are typically not simultaneously diagonalizable for all i. Comparing (9), (12) and (15) we then get the following instructive inclusion relations

$$\mathcal{D}_0 \subseteq \mathcal{D}_{\mathrm{cl}} \subseteq \mathcal{D}_{\mathrm{sep}}. \tag{16}$$

Thanks to the underlying geometric picture—which provides a unified basis for quantifying the different correlation types—this can directly be translated into relations between the respective measures

$$I(\rho) \geqslant Q(\rho) \geqslant E(\rho). \tag{17}$$

Finally, we present the classical counterpart of (15), the classical correlation. To motivate its measure we first rewrite (15) as [66]

$$Q(\rho) = \min_{\{P_A^{(i)}\},\{P_B^{(j)}\}} S\left(\rho \| \sum_{ij} P_A^{(i)} \otimes P_B^{(j)} \rho P_A^{(i)} \otimes P_B^{(j)}\right) \tag{18}$$

where $\{P_A^{(i)}\}$ and $\{P_B^{(j)}\}$ are two projective measurements, satisfying $\left(P_{A/B}^{(i)}\right)^2 = P_{A/B}^{(i)}$ and $\sum_i P_{A/B}^{(i)} = \mathbb{1}_{A/B}$. The closest classical state χ_ρ is then the state resulting from ρ after the optimal projective measurements has been performed. Accordingly, the total correlation in χ_ρ is then nothing else than the classical correlation in ρ [51]

$$C(\rho) \equiv I(\chi_\rho). \tag{19}$$

Since quantum states cannot be dissected into classical and quantum parts in a strict mathematical sense, it is not surprising that our measures do typically not obey the relation $I = Q + C$. However, this exact additive relation is valid whenever the closest classical state χ_ρ and the closest uncorrelated state π_ρ have the same eigenstates. For a simple proof of this statement see appendix A.

2.3. Application to systems of electrons

In this section, we will discuss how the previously defined QI concepts are adopted to electronic structure theory. For this, we need to establish in a first step a notion of subsystems in fermionic quantum systems and also learn how to deal with related conceptual peculiarities. All these aspects are absolutely vital for establishing a QI framework for quantifying in an operationally meaningful way total, quantum and classical correlation and entanglement in molecular ground states.

We start by assigning a reference basis to the one-particle Hilbert space $\mathcal{H}^{(1)} = \mathcal{H}_l^{(1)} \otimes \mathcal{H}_s^{(1)}$, by referring to a set of orthonormal spin-orbitals $\{|\chi_i\rangle \otimes |\sigma\rangle\}_{i=1}^{D}$, with $|\chi_i\rangle \in \mathcal{H}_l^{(1)}$ being the orbital state and $\sigma \in \{\uparrow,\downarrow\}$ describing the spin degree of freedom. The corresponding Fock space $\mathcal{F}[\mathcal{H}^{(1)}]$ is then spanned by the configuration states

$$|n_{1\uparrow}, n_{1\downarrow}, \ldots, n_{D\downarrow}\rangle \equiv \left(f^{\dagger}_{\chi_1\uparrow}\right)^{n_{1\uparrow}} \ldots \left(f^{\dagger}_{\chi_D\downarrow}\right)^{n_{D\downarrow}} |\Omega\rangle\,. \tag{20}$$

Here, $f^{(\dagger)}_{\chi_i\sigma}$ denotes the annihilation (creation) operator associated to the spin-orbital $|\chi_i\rangle \otimes |\sigma\rangle$. They satisfy the fermionic anti-commutation relations $\{f^{(\dagger)}_{\chi_i\sigma}, f^{(\dagger)}_{\chi_j\sigma'}\} = 0$ and $\{f^{\dagger}_{\chi_i\sigma}, f_{\chi_j\sigma'}\} = \delta_{i,j}\delta_{\sigma,\sigma'}\mathbb{1}$, with $\{A, B\} \equiv AB + BA$, and $|\Omega\rangle$ is the vacuum state. With respect to the ordered basis $\{|\chi_i\rangle \otimes |\sigma\rangle\}_{i=1}^{D}$, we now establish the notion of subsystems. For the purpose of this paper, we focus primarily on the partitioning of orbitals $\{|\chi_i\rangle\}$ into two subsets A and B. This means effectively to divide the orbital one-particle Hilbert space into two complementary subspaces of dimensions $D_{A/B}$, $\mathcal{H}_l^{(1)} = \mathcal{H}_{l,A}^{(1)} \oplus \mathcal{H}_{l,B}^{(1)}$ and thus $\mathcal{H}^{(1)} = \mathcal{H}_A^{(1)} \oplus \mathcal{H}_B^{(1)}$ where $\mathcal{H}_{A/B}^{(1)} \equiv \mathcal{H}_{l,A/B}^{(1)} \otimes \mathcal{H}_s^{(1)}$. This splitting in turn induces a tensor-product decomposition on the Fock state,

$$\mathcal{F}[\mathcal{H}_A^{(1)} \oplus \mathcal{H}_B^{(1)}] \cong \mathcal{F}[\mathcal{H}_A^{(1)}] \otimes \mathcal{F}[\mathcal{H}_B^{(1)}], \tag{21}$$

through the map

$$\begin{aligned} &|n_{1\uparrow}, n_{1\downarrow}, \ldots, n_{D_A\downarrow}, n_{D_{A+1}\uparrow}, \ldots, n_{D\downarrow}\rangle \mapsto \\ &\quad |n_{1\uparrow}, n_{1\downarrow}, \ldots, n_{D_A\downarrow}\rangle \otimes |n_{D_{A+1}\uparrow}, , \ldots, n_{D\downarrow}\rangle. \end{aligned} \tag{22}$$

It is important to note, however, that such a tensor-product decomposition does not hold on the level of fermionic operators that are defined within the respective subsystems. This is clear from the observation that the creation and annihilation operators associated with spin-orbitals in subsystem A and B do not commute with each other, and, as a result, cannot be considered local observable operators. The immediate consequences is the violation of special relativity, exemplified by the possibility of superluminal signaling [67, 68]. We resolve this by invoking the fermionic parity superselection rule [33, 69] (P-SSR). The P-SSR excludes observables that do not commute with the local particle number parity operator $\hat{\mathcal{P}}^{(A/B)} = \hat{P}^{(A/B)}_{\text{even}} - \hat{P}^{(A/B)}_{\text{odd}}$, where $\hat{P}^{A/B}_{\tau}$ is the projection onto the $\tau \in \{\text{even,odd}\}$ parity subspace acting on subsystem A/B. As a result, the accessible correlation and entanglement in a bipartite state ρ_{AB} is reduced to those in the superselected state [68, 70]

$$\rho^{\text{P}}_{AB} = \sum_{\tau,\tau'=\text{even, odd}} \hat{P}^{(A)}_{\tau} \otimes \hat{P}^{(B)}_{\tau'} \rho_{AB} \hat{P}^{(A)}_{\tau} \otimes \hat{P}^{(B)}_{\tau'}, \tag{23}$$

since, from an operational point of view, ρ_{AB} and ρ^{P}_{AB} are equivalent. To summarize, the correlation quantities $X = I, C, Q, E$ defined in section 2.2 under P-SSR can be calculated as

$$X^{\text{P}}(\rho_{AB}) = X(\rho^{\text{P}}_{AB}). \tag{24}$$

When the creation or annihilation of *pairs* of particles is also not possible, this results in an even more restrictive particle number superselection rules [33, 71] (N-SSR). In this case we simply replace ρ^{P}_{AB} in (24) with the N-SSR superselected state

$$\rho^{\text{N}}_{AB} = \sum_{m=0}^{2D_A} \sum_{n=0}^{2D_B} P^{(A)}_m \otimes P^{(B)}_n \rho_{AB} P^{(A)}_m \otimes P^{(B)}_n, \tag{25}$$

where $P^{(A/B)}_m$ is the projection onto the m-particle subspace acting on subsystem A/B.

We remark that if one is only interested in the numerical structure of the quantum state, it is possible to quantify correlation and entanglement without SSR, simply by mapping the fermionic state to that of a spin system via the respective Jordan–Wigner transformation. By contrast, if the orbital entanglement in the molecules is to be accessed or utilized, e.g. through an entanglement swapping protocol from molecule to quantum registers, the inclusion of SSR is operationally crucial. Accessing orbital entanglement requires measurement or more generally operations to be performed on the orbitals, which are limited precisely by the SSR. Although at the moment, perfect control over every element within a molecule or arbitrary operations on orbitals is not yet possible, this status may greatly improve soon with the on-going second

quantum revolution [72]. If SSR are ignored, one would grossly overestimate the accessible correlation and entanglement.

Finally, we introduce the primary objects of interests, namely the one- and two-*orbital* reduced density matrices (RDMs). Formally, the one- and two-orbital RDMs of a pure state $|\Psi\rangle$ are defined via the following requirements

$$\rho_i : \mathrm{Tr}[\rho_i \hat{\mathcal{O}}] = \langle \Psi|\hat{\mathcal{O}}|\Psi\rangle, \quad \forall \hat{\mathcal{O}} \in \mathcal{A}_i \tag{26a}$$

$$\rho_{i,j} : \mathrm{Tr}[\rho_{ij} \hat{O}] = \langle \Psi|\hat{\mathcal{O}}|\Psi\rangle, \quad \forall \hat{\mathcal{O}} \in \mathcal{A}_{ij}. \tag{26b}$$

In practice, they are computed from partial two- and four-*particle* RDMs [73], respectively. Exploiting the symmetry of the overall quantum state reduces further the computational cost [24]. For example, it is common to restrict the calculation of the molecular ground state to a predefined, fixed particle number N and spin magnetization m_S (for a given spin state $2S+1$). Consequently, the one- and two-orbital RDM can only be mixtures of fixed electron-number and magnetization states. In other words, the one-orbital RDM is diagonal in the fixed particle number and magnetization basis

$$\rho_i = \begin{pmatrix} \langle f_{i\uparrow} f_{i\uparrow}^\dagger f_{i\downarrow} f_{i\downarrow}^\dagger \rangle & 0 & 0 & 0 \\ 0 & \langle f_{i\uparrow}^\dagger f_{i\uparrow} f_{i\downarrow} f_{i\downarrow}^\dagger \rangle & 0 & 0 \\ 0 & 0 & \langle f_{i\uparrow} f_{i\uparrow}^\dagger f_{i\downarrow}^\dagger f_{i\downarrow} \rangle & 0 \\ 0 & 0 & 0 & \langle f_{i\uparrow}^\dagger f_{i\uparrow} f_{i\downarrow}^\dagger f_{i\downarrow} \rangle \end{pmatrix} \tag{27}$$

and the two-orbital RDM is block diagonal, the form of which we refer to [24].

3. Analytical examples

In this section we demonstrate with two analytic examples (a) the strong influence of SSR on the accessible correlation and entanglement and (b) the subtle connection between entanglement and chemical bonding.

3.1. Single electron state

We consider a single polarized electron within the manifold of two orbitals A and B. The state of the electron is then simply a superposition of the form

$$|\Psi(\theta,\varphi)\rangle = \cos(\theta)|1_A, 0_B\rangle + e^{i\varphi}\sin(\theta)|0_A, 1_B\rangle, \tag{28}$$

where $|n_A, n_B\rangle \equiv (f_A^\dagger)^{n_A}(f_B^\dagger)^{n_B}|\Omega\rangle$ are local occupation number eigenstates, and $\theta \in [0,\pi)$, $\varphi \in [0, 2\pi)$. Such a state belongs to the one-particle Hilbert space $\mathcal{H}^{(1)}$ isomorphic to that of a single qubit, which is a subspace of the four-dimensional total Fock space $\mathcal{F}[\mathcal{H}^{(1)}]$. Referring to the tensor product between the two local Fock spaces $\mathcal{F}[\mathcal{H}^{(1)}] = \mathcal{F}[\mathcal{H}_A^{(1)}] \otimes \mathcal{F}[\mathcal{H}_B^{(1)}]$, the density operator $\rho(\theta,\varphi)$ is given in the basis $|0_A, 0_B\rangle, |1_A, 0_B\rangle, |0_A, 1_B\rangle, |1_A, 1_B\rangle$ by,

$$\rho(\theta,\varphi) = |\Psi(\theta,\varphi)\rangle\langle\Psi(\theta,\varphi)| = \begin{pmatrix} 0 & 0 & 0 & 0 \\ 0 & \cos^2(\theta) & \frac{e^{i\varphi}}{2}\sin(2\theta) & 0 \\ 0 & \frac{e^{-i\varphi}}{2}\sin(2\theta) & \sin^2(\theta) & 0 \\ 0 & 0 & 0 & 0 \end{pmatrix}. \tag{29}$$

Since $\rho(\theta,\varphi)$ is pure (cf equation (2)), the associated entanglement E and quantum correlation Q are the same, and so are the closest separable χ_ρ and classical states σ_ρ, respectively. The closest product state π_ρ as well as the classical and separable states (in this case they coincide) χ_ρ to $\rho(\theta,\varphi)$ is diagonal in this basis with

$$\begin{aligned} \mathrm{diag}(\pi_\rho) &= \left(\cos^4(\theta), \frac{1}{4}\sin^4(2\theta), \frac{1}{4}\sin^4(2\theta), \sin^4(\theta)\right), \\ \mathrm{diag}(\chi_\rho) &= \left(0, \cos^2(\theta), \sin^2(\theta), 0\right). \end{aligned} \tag{30}$$

Moreover, the total correlation I, quantum correlation Q, classical correlation C, and entanglement E of $\rho(\theta,\varphi)$ are given by

$$\begin{aligned} \frac{1}{2}I(\rho) &= Q(\rho) = C(\rho) = E(\rho) \\ &= -[\cos^2(\theta)\ln(\cos^2(\theta)) + \sin^2(\theta)\ln(\sin^2(\theta))] \\ &\equiv P(\theta). \end{aligned} \tag{31}$$

Table 1. Total correlation I, classical correlation C, quantum correlation Q, and entanglement E between the two orbitals A and B in the single electron state (28), for the case without SSR and with P/N-SSR.

	I	C	Q	E
No SSR	$2P(\theta)$	$P(\theta)$	$P(\theta)$	$P(\theta)$
P/N-SSR	$P(\theta)$	$P(\theta)$	0	0

In the presence of a SSR, the superselected state loses all coherence between different local particle number sectors

$$\rho^{\mathrm{P,N}}(\theta,\varphi) = \cos^2(\theta)|1_A,0_B\rangle\langle 1_A,0_B| + \sin^2(\theta)|0_A,1_B\rangle\langle 0_A,1_B|. \tag{32}$$

As can be easily seen from its form in equation (32), the superselected state $\rho^{\mathrm{P,N}}(\theta,\varphi)$ is separable, since it can be written as a simple mixture of product states. Furthermore, it is also classical since it is diagonal in a product basis. From this it follows, that all correlation in (32) between the two orbitals are classical. We summarize all correlation quantities with and without SSRs in table 1.

3.2. Single covalent bond

In this example, we apply the same QI concepts as in the previous section now to a pair of bonding electrons in a hydrogen-like diatomic molecule, described by the state

$$|\Psi\rangle = f^\dagger_{\phi\uparrow} f^\dagger_{\phi\downarrow}|\Omega\rangle\ . \tag{33}$$

Here, ϕ is the bonding orbital, formed by superimposing two 1 s-like orbitals on the two nuclear centers L (left) and R (right)

$$\phi = \mathcal{N}(\varphi_L + \varphi_R) \tag{34}$$

where $\mathcal{N}$ is a normalizing constant.

Before we are able to proceed with a calculation of the correlation in $|\Psi\rangle$, being it quantum or classical, we first have to decide on a choice of orbital splitting. An obvious choice would be to consider the correlation between the bonding orbital ϕ and the corresponding anti-bonding orbital $\overline{\phi} = \overline{\mathcal{N}}(\varphi_L - \varphi_R)$. Together ϕ and $\overline{\phi}$ form a minimal active space, within which we will perform all our entanglement analysis. Referring to the splitting between ϕ and $\overline{\phi}$, $|\Psi\rangle$ is clearly a product state. As a result, it has zero correlation and entanglement. While this finding seems odd at first sight, as one would expect a considerable amount of entanglement to be 'stored' in a chemical bond, let us next consider a different, seemingly less intuitive alternate choice of the splitting.

In the top panel of figure 2, we illustrate the formation of the bonding orbital ϕ from the two local 1 s-type orbitals φ_L and φ_R, respectively. We then make a cut at the center of the molecule dividing the space into left and right half, and project the bonding orbital onto the two half-spaces (central panel), denoted as ϕ_L and ϕ_R. After normalization, the resulting two-electron wave function (33) can be written as

$$\begin{aligned}|\Psi\rangle &= \frac{1}{2}(f^\dagger_{\phi_L\uparrow} + f^\dagger_{\phi_R\uparrow})(f^\dagger_{\phi_L\downarrow} + f^\dagger_{\phi_R\downarrow})|\Omega\rangle \\ &= \frac{1}{2}(f^\dagger_{\phi_L\uparrow} f^\dagger_{\phi_L\downarrow} + f^\dagger_{\phi_R\uparrow} f^\dagger_{\phi_R\downarrow} + f^\dagger_{\phi_L\uparrow} f^\dagger_{\phi_R\downarrow} - f^\dagger_{\phi_L\downarrow} f^\dagger_{\phi_R\uparrow})|\Omega\rangle.\end{aligned} \tag{35}$$

Hence, with respect to a splitting between the left and right projected orbitals ϕ_L and ϕ_R, simple calculations lead to a set of entirely different values of correlation quantities of $\rho = |\Psi\rangle\langle\Psi|$

$$\frac{1}{2}I(\rho) = Q(\rho) = C(\rho) = E(\rho) = 2\ln 2. \tag{36}$$

When SSR are considered, P-SSR and N-SSR eliminate coherent terms between different local parity and particle number sectors, respectively, leading to superselected states of the form

$$\begin{aligned}\rho^{\mathrm{P}} &= \frac{1}{2}|\Psi_{\mathrm{even}}\rangle\langle\Psi_{\mathrm{even}}| + \frac{1}{2}|\Psi_{\mathrm{odd}}\rangle\langle\Psi_{\mathrm{odd}}| \\ \rho^{\mathrm{N}} &= \frac{1}{4}|\Psi_{2,0}\rangle\langle\Psi_{2,0}| + \frac{1}{4}|\Psi_{0,2}\rangle\langle\Psi_{0,2}| \\ &\quad + \frac{1}{2}|\Psi_{1,1}\rangle\langle\Psi_{1,1}|,\end{aligned} \tag{37}$$

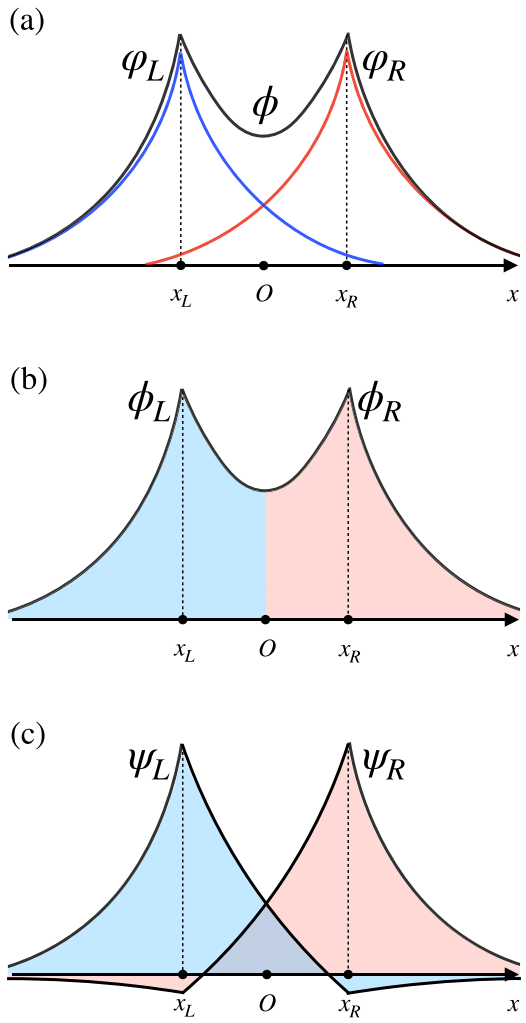

Figure 2. (a) Formation of the (up to normalization) bonding orbital ϕ with two local atomic 1 s-type orbitals φ_L and φ_R with nuclear centers at $x_{L,R}$. (b) Projection of the bonding orbital onto the left and right half space. (c) Rotated bonding and anti-bonding orbitals ψ_L and ψ_R.

where

$$\begin{aligned}
|\Psi_{\text{odd}}\rangle &= |\Psi_{1,1}\rangle = \frac{1}{\sqrt{2}}\left(f^\dagger_{\phi_L\uparrow}f^\dagger_{\phi_R\downarrow} - f^\dagger_{\phi_L\downarrow}f^\dagger_{\phi_R\uparrow}\right)|\Omega\rangle,\\
|\Psi_{\text{even}}\rangle &= \frac{1}{\sqrt{2}}\left(f^\dagger_{\phi_L\uparrow}f^\dagger_{\phi_L\downarrow} + f^\dagger_{\phi_R\uparrow}f^\dagger_{\phi_R\downarrow}\right)|\Omega\rangle\\
|\Psi_{2,0}\rangle &= f^\dagger_{\phi_L\uparrow}f^\dagger_{\phi_L\downarrow}|\Omega\rangle,\\
|\Psi_{0,2}\rangle &= f^\dagger_{\phi_R\uparrow}f^\dagger_{\phi_R\downarrow}|\Omega\rangle.
\end{aligned} \tag{38}$$

In this case both P- and N-SSR reduce quantum correlation as well as entanglement by 50% and 75%, respectively, while at the same time having no effect on the classical correlation. Consequently, the total correlation is lowered by the same amount of decrease in the quantum correlation, as the relation $I = C + Q$ holds in this case. We summarize the correlation quantities with and without SSRs in table 2.

This example already illustrates that, by referring to a suitable orbital splitting that allows to capture a certain degree of spatial locality, one can recover strong correlation as one would expect in a chemical bond. Although the above choice of splitting seems from a QI perspective to be reasonable in terms of recovering correlation effects, it requires an artificial cut of the bonding orbital into two halves. Moreover, from the resulting orbitals ϕ_L and ϕ_R, one cannot recover the anti-bonding orbital $\overline{\phi} \propto \varphi_L - \varphi_R$. As a matter of fact, $\{\phi_L, \phi_R\}$ do not span the same Hilbert space as the two local atomic orbitals $\{\varphi_L, \varphi_R\}$. Therefore the optimal approach must include in addition the anti-bonding orbital into the total Hilbert space $\overline{\phi} = \overline{N}(\varphi_L - \varphi_R)$. To explore all possible choices of orbital bases, we unitarily (assuming for simplicity but without loss of

Table 2. Total correlation, classical correlation, quantum correlation, and entanglement between the bonding and anti-bonding orbitals in single bond state $|\Psi\rangle$ in (33) (top panel), and between the two projected orbitals in the same state $|\Psi\rangle$ re-expressed in (35) (bottom panel), for the case without SSR, with P- and N-SSR.

$\phi, \overline{\phi}$	I	C	Q	E
No SSR	0	0	0	0
P, N-SSR	0	0	0	0
ϕ_L, ϕ_R	I	C	Q	E
No SSR	$4\ln 2$	$2\ln 2$	$2\ln 2$	$2\ln 2$
P-SSR	$3\ln 2$	$2\ln 2$	$\ln 2$	$\ln 2$
N-SSR	$\frac{5}{2}\ln 2$	$2\ln 2$	$\frac{1}{2}\ln 2$	$\frac{1}{2}\ln 2$

generality real coefficients) transform the orbitals ϕ, $\overline{\phi}$

$$\begin{aligned} \psi_L &= \cos(\theta)\phi + \sin(\theta)\overline{\phi}, \\ \psi_R &= -\sin(\theta)\phi + \cos(\theta)\overline{\phi}. \end{aligned} \tag{39}$$

After this unitary basis rotation, we can rewrite the state $|\Psi\rangle$ in equation (33) as

$$\begin{aligned} |\Psi\rangle = \Big[&\cos^2(\theta) f^\dagger_{\psi_L\uparrow} f^\dagger_{\psi_L\downarrow} + \sin^2(\theta) f^\dagger_{\psi_R\uparrow} f^\dagger_{\psi_R\downarrow} \\ &+ \cos(\theta)\sin(\theta)\left(f^\dagger_{\psi_L\uparrow} f^\dagger_{\psi_R\downarrow} - f^\dagger_{\psi_L\downarrow} f^\dagger_{\psi_R\uparrow}\right)\Big]|\Omega\rangle. \end{aligned} \tag{40}$$

The entanglement of $\rho = |\Psi\rangle\langle\Psi|$ is simply

$$\begin{aligned} E(\rho) &= -2\left[\cos^2(\theta)\ln(\cos^2(\theta)) + \sin^2(\theta)\ln(\sin^2(\theta))\right] \\ &= 2P(\theta). \end{aligned} \tag{41}$$

From equation (41) it follows that maximal entanglement is realized by a rotation with angle $\theta = \frac{\pi}{4}$. As can be seen from table 2, in the latter basis the resulting $E(\rho)$ reaches also $2\ln 2$, in perfect agreement with the case of the artificial half-splitting discussed previously. Moreover, assuming a rotation of $\theta = \frac{\pi}{4}$, the transformed orbitals ψ_L and ψ_R, illustrated in the bottom panel (c) of figure 2, are simply equal superpositions of the initial bonding ϕ and anti-bonding $\overline{\phi}$ orbitals, with plus and minus signs respectively. As a matter of fact, the final expression for the state in equation (40), expressed in the basis $\{\psi_L, \psi_R\}$, takes the same form as its counterpart in equation (35), with the replacement $\psi_{L,R} \to \phi_{L,R}$. Therefore, in the particular choice of $\theta = \frac{\pi}{4}$, we find that all correlation quantities (with or without SSRs) of the state given by equation (40) coincide with those of the state in equation (35). Thus, we can interpret the rotation angle $\theta = \frac{\pi}{4}$ as the point where maximal orbital localization effect is achieved, while still keeping the orbitals orthogonal and without dissecting them.

To explore more comprehensively the connection between orbital entanglement and chemical bonding, let us consider the cases of maximal and minimal entanglement in some prototypical states of definite bond order. In MO theory, the bond order of a state is defined as the difference in the occupation number between the bonding orbital ϕ and its anti-bonding orbital partner $\overline{\phi}$ divided by 2 [74]

$$\text{bond order} = \frac{1}{2}(N_{\text{bond}} - N_{\text{antibond}}). \tag{42}$$

To illustrate the concept of a bond order we consider the following four states

$$\begin{aligned} |\Psi_1\rangle &= f^\dagger_{\phi\uparrow}|\Omega\rangle, \\ |\Psi_2\rangle &= f^\dagger_{\phi\uparrow} f^\dagger_{\phi\downarrow}|\Omega\rangle, \\ |\Psi_3\rangle &= f^\dagger_{\phi\uparrow} f^\dagger_{\phi\uparrow} f^\dagger_{\overline{\phi}\uparrow}|\Omega\rangle, \\ |\Psi_4\rangle &= f^\dagger_{\phi\uparrow} f^\dagger_{\phi\downarrow} f^\dagger_{\overline{\phi}\uparrow} f^\dagger_{\overline{\phi}\downarrow}|\Omega\rangle, \end{aligned} \tag{43}$$

which have a bond order of $\frac{1}{2}$, 1, $\frac{1}{2}$, and 0, respectively, according to (42). We can easily find the minimal entanglement of all four states to be zero, with respect to the orbital partition between ϕ and $\overline{\phi}$, that is, the bonding and anti-bonding orbitals. Under an arbitrary orbital rotation of angle θ

$$\begin{aligned} f^\dagger_{\psi_L\sigma} &= \cos(\theta) f^\dagger_{\phi\sigma} + \sin(\theta) f^\dagger_{\overline{\phi}\sigma}, \\ f^\dagger_{\psi_R\sigma} &= \sin(\theta) f^\dagger_{\phi\sigma} - \cos(\theta) f^\dagger_{\overline{\phi}\sigma}, \end{aligned} \tag{44}$$

Table 3. Bond order, maximal and minimal entanglement of the four states given in equation (43).

$\bar{\phi}$	—	—	↑	↑↓
ϕ	↑	↑↓	↑↓	↑↓
	$\|\Psi_1\rangle$	$\|\Psi_2\rangle$	$\|\Psi_3\rangle$	$\|\Psi_4\rangle$
Bond order	$\frac{1}{2}$	1	$\frac{1}{2}$	0
$E_{\max}$	$\ln 2$	$2\ln 2$	$\ln 2$	0
$E_{\min}$	0	0	0	0

the four states transform to

$$
\begin{aligned}
|\Psi_1\rangle &= \cos(\theta) f^\dagger_{\psi_L\uparrow}|\Omega\rangle + \sin(\theta) f^\dagger_{\psi_R\uparrow}|\Omega\rangle,\\
|\Psi_2\rangle &= \cos^2(\theta) f^\dagger_{\psi_L\uparrow} f^\dagger_{\psi_L\downarrow}|\Omega\rangle + \sin^2(\theta) f^\dagger_{\psi_R\downarrow} f^\dagger_{\psi_R\downarrow}|\Omega\rangle\\
&\quad \times \cos(\theta)\sin(\theta)\left(f^\dagger_{\psi_L\uparrow} f^\dagger_{\psi_R\downarrow} - f^\dagger_{\psi_L\downarrow} f^\dagger_{\psi_R\uparrow}\right)|\Omega\rangle,\\
|\Psi_3\rangle &= f^\dagger_{\psi_L\uparrow}\left(\cos(\theta) f^\dagger_{\psi_L\downarrow} f^\dagger_{\psi_R\uparrow} - \sin(\theta) f^\dagger_{\psi_R\uparrow} f^\dagger_{\psi_R\downarrow}\right)|\Omega\rangle,\\
|\Psi_4\rangle &= f^\dagger_{\psi_L\uparrow} f^\dagger_{\psi_L\downarrow} f^\dagger_{\psi_R\uparrow} f^\dagger_{\psi_R\downarrow}|\Omega\rangle.
\end{aligned}
$$

The latter shows that the resulting entanglement E with respect to the partition between ψ_L and ψ_R of $|\Psi_{1,2,3}\rangle$ is maximized for $\theta = \frac{\pi}{4}$, whereas the entanglement of $|\Psi_4\rangle$ remains invariant under orbital transformation. To summarize these findings we compile in table 3 the maximal and minimal entanglement of these four states as a function of the bond order. Remarkably, we find that the maximal entanglement, realized between the maximally localized orbitals, is *indeed* proportional to the bond order (42) of each state. A single bond of bond order 1 thus corresponds to the entanglement value $E = 2\ln 2$ between the fully-localized atomic-like orbitals. Intriguingly, this value exceeds by an order of magnitude the numbers reported in previous studies [19–28]. In turn, this clearly demonstrates that QI tools applied to delocalized orbitals describe primarily the validity of the independent electron-pair picture rather than the bonding structure of molecular systems.

Lastly, we remark that the insights we gained from the single covalent bond states extends beyond bonds of order 1. Namely, for a prototypical K-fold bond state $|\Psi_K\rangle = \prod_{k=1}^{K} f^\dagger_{\phi_k\uparrow} f^\dagger_{\phi_k\downarrow}|0\rangle$, rotating pairs of bonding and antibonding orbitals ϕ_k and $\bar{\phi}_k$ by $\pi/4$ leads to K pairs of maximally entangled rotated orbitals, amounting to $K(2\ln 2)$ of total orbital–orbital entanglement.

4. Computational details

In section 5, we will analyze and decompose electron-correlation effects into its classical and quantum correlation as well as entanglement contributions at the example of a few chain-like and cyclic π-conjugated organic molecules in their electronic ground state, namely, ethylene (C_2H_4), decapentaene ($C_{10}H_{12}$), eicosadecaene ($C_{20}H_{22}$), and benzene (C_6H_6). In this preceding section, we will present the computational details of our ground state calculation, as well as an algorithm for numerically obtaining the quantum correlation.

4.1. General considerations

For each molecular compound, the geometrical parameters were taken from literature and are listed as *xyz* coordinates in the appendix (see tables B1–B4). Since our primary focus will be on rationalizing the chemical bonding as well as electron correlation effects that originate from the π-subspace of the above mentioned conjugated systems, we carried out complete-active-space (CAS) calculations correlating n_e electrons in n_o π-orbitals. In this particular case it follows that $n_e = n_o$ which in turn equals the number of carbon atoms in the molecule. Hence, by choice, our analysis neglects in the present work any electron correlation contributions arising from σ-type MOs as well as set(s) of higher-lying (correlating) secondary π^*-orbitals. To corroborate this approximation, we performed additional test calculations on decapentaene considering CAS spaces of CAS(34,34) and CAS(10,20), respectively. Those large-scale test calculations revealed that correlation contributions to the valence π-π^*-space arising either from the C–C and C–H σ-space (CAS(34,34)) or from additional correlating π^*-orbitals (CAS(10,20)) are (a) differential (within the additional sets of $\{\sigma, \sigma^*\}$ MOs) or (b) safely negligible with natural orbital occupation numbers of the valence π-π^*-space changing by less than ± 0.003.

All quantum-chemical calculations, except for the density matrix renormalization group (DMRG) calculations [75–77] (for a recent review of DMRG in QC, see for example [78]) further described below, were performed with the 2019 version of the MOLPRO software package [79–81]. By making use of the

FCIDUMP file format [82] in MOLPRO, we exported the (effective) one- and two-electron Hamiltonian integrals in a given MO basis for the ensuing matrix product state (MPS) wave function optimization within the DMRG software QCMAQUIS [83–85]. All calculations were carried out in C_1 point group symmetry as well as with correlation-consistent Dunning-type basis sets [86] of double-ζ quality (cc-pVDZ). The latter one-particle basis set should be sufficiently large to provide a qualitatively correct description of the valence correlation effects, in particular of the π-bonds. In order to critically assess the correlation contributions introduced in section 2.2 within the π-space manifold of our molecular systems, we considered three distinct set of MOs that are related to each other by suitable orbital rotations. To this end, we first performed self-consistent field Hartree–Fock (HF) calculations for the spin-singlet ($S=0$) ground state of each molecule, yielding a set of *canonical* HF MOs for the respective molecular systems. In an ensuing step, we then applied a Pipek–Mezey (PM) [87] localization procedure which yields a second set of *localized* MOs (dubbed as 'PM-localized' in the following) while retaining the σ- and π-character of the initial canonical MOs, respectively. It should be emphasized that, although it is possible to perform the PM-localization on the entire set of canonical MOs [25], in this work the PM-localization is implemented separately within the bonding (occupied) and antibonding (virtual) orbital sub-manifolds, as it is common practice in the QC community. The final set of *atomic-like* of orbitals was obtained by means of a (sequence of) 2×2 Jacobi-rotation(s) by an angle θ within the π-space manifold and setting out either from the PM-localized MO basis (ethylene and polyenes) or the canonical MO basis (benzene). In the former, a single rotation by $\theta=\frac{\pi}{4}$ within a pair of bonding π and its antibonding partner π^* suffices to yield the desired atomic-like molecular basis. It is worthwhile to mention that the latter scheme was recently also explored in an attempt to reduce the 1-norm of the Hamiltonian in the context of quantum computing applications [88]. In contrast to the remaining molecules studied in this work, obtaining an atomic-like orbital basis for benzene requires in general six-orbital unitary transformations, which can be decomposed into three consecutive sets of pairwise rotations (see appendix C).

In order to (approximately) solve the full CI problem for a given CAS orbital space, we employed a spin-adapted DMRG algorithm [84] as implemented in QCMAQUIS [83–85]. Having thus obtained an optimized MPS wave function for the singlet electronic ground state, the latter was then used to compute the one- and two-*orbital* RDMs which are the primary input quantities for the correlation measures defined in section 2.2. In all DMRG calculations we employed a two-site optimization algorithm starting from a HF guess (`init_guess = hf` in QCMAQUIS) for the initial MPS while varying the maximum number of renormalized block states m from $m=500$ up to $m=2000$ until the total energy was converged to at least less than sub-μ Hartree accuracy. Furthermore, all DMRG calculations were carried out with an orbital ordering of pairwise correlating π-π^*-orbitals.

For the orbital visualizations we made use of JMOL [89]. To aid the reader's visual guide, we applied for each molecular system individual isosurface thresholds as indicated in the figures.

4.2. Numerical calculation of quantum correlation

The set of classically correlated states (14) has a complicated and highly non-convex structure, which makes an optimization over it a formidable task. Fortunately, [51] provides a suitable theorem that connects the spectrum of the closest classical state χ_ρ to the diagonal entries of ρ in the eigenbasis of χ_ρ. More precisely, if $\chi_\rho=\sum_{ij}\lambda_{ij}|i\rangle\langle i|\otimes|j\rangle\langle j|$ is the closest classical state to ρ, then its spectrum is given by

$$\lambda_{ij}=\langle i|\otimes\langle j|\,\rho\,|i\rangle\otimes|j\rangle. \tag{45}$$

In other words, the closest classical state to ρ is of the form

$$\chi_\rho=\sum_{ij}|i\rangle\langle i|\otimes|j\rangle\langle j|\rho|i\rangle\langle i|\otimes|j\rangle\langle j|. \tag{46}$$

This finding represents the starting point for our quest to search for the optimal local bases $\{|i\rangle\}$ and $\{|j\rangle\}$ of two subsystems A and B, respectively, recovering the minimizer of (15). Given that any two bases can be connected by a unique unitary operator $U|i\rangle\mapsto|i'\rangle$, provided that we fix the local computational bases, this search is then equivalent to finding the optimal unitary operators U_A and U_B for the respective subsystems. In the following we present a random walk algorithm assisted by probabilistic rejection, in search for the optimal local unitary operators U_A and U_B within the manifolds of local unitaries $\mathcal{U}_A$ and $\mathcal{U}_B$, respectively.

Algorithm 1. Calculating quantum correlation.

INPUT: bipartite quantum state ρ
OUTPUT: $Q(\rho)$ and the closest classical state χ_ρ to ρ
COMPUTATION:
SET initial local bases $\{|i^{(0)}\rangle_A\}$ and $\{|j^{(0)}\rangle_B\}$;
SET $n=0$ and $U_A^{(0)} = U_B^{(0)} = \mathbb{1}$;
COMPUTE $\chi_\rho^{(0)} = \sum_{ij} |i^{(0)}\rangle\langle i^{(0)}| \otimes |j^{(0)}\rangle\langle j^{(0)}| \rho |i^{(0)}\rangle\langle i^{(0)}| \otimes |j^{(0)}\rangle\langle j^{(0)}|$;
COMPUTE $Q(\rho)^{(0)} = S(\rho||\chi_\rho^{(0)})$;
WHILE $n < N_{\text{step}}$ **DO**:
  SAMPLE random unitary matrices $V_{A,B}$;
  COMPUTE $V_{A,B} \leftarrow V_{A,B}^{\frac{1}{M}}$;
  UPDATE $U_{A,B}^{(n+1)} \leftarrow V_{A,B} U_{A,B}^{(n)}$;
  COMPUTE new local bases
    $U_A^{(n+1)}|i^{(n)}\rangle \mapsto |i^{(n+1)}\rangle$, $U_B^{(n+1)}|j^{(n)}\rangle \mapsto |j^{(n+1)}\rangle$
  COMPUTE new classical state
    $\chi_\rho^{(n+1)} = \sum_{ij} |i\rangle\langle i| \otimes |j\rangle\langle j| \rho |i\rangle\langle i| \otimes |j\rangle\langle j|$;
  COMPUTE $Q^{(n+1)} = S(\rho||\chi^{(n+1)})$;
  SAMPLE uniformly $p \in (0, 1]$;
  IF $Q^{(n+1)} < Q^{(n)}$:
    UPDATE $Q(\rho) \leftarrow Q^{(n)}(\rho)$;
    UPDATE $\chi_\rho \leftarrow \chi_\rho^{(n)}$;
    UPDATE $n \leftarrow n+1$;
END

The computational scheme outlined in Algorithm 1 consists of the following steps: One first initializes a pair of local bases sets $\{|i^{(0)}\rangle\}$ and $\{|j^{(0)}\rangle\}$ for the two subsystems as well as the two local unitary operators as $U_{A,B}^{(0)} = \mathbb{1}$. The initial bases determine a candidate for the closest classical state $\chi_\rho^{(0)}$ according to (46) and the distance $Q^{(0)} = S(\rho||\chi_\rho^{(0)})$. The unitary operators live on the connected manifolds $\mathcal{U}_{A,B} \ni U_{A,B}$ which allows us to make use of a random walk algorithm to find the optimal set of unitary operators. We start by performing a small step in $\mathcal{U}_{A,B}$ by multiplying $U_{A,B}^{(0)}$ with a 'small' unitary operator $V_{A,B}$ close to the identity, arriving at $U_{A,B}^{(1)}$, which, in turn, determines a pair of local bases $U_A^{(1)}|i^{(0)}\rangle \equiv |i^{(1)}\rangle$, $U_B^{(1)}|j^{(0)}\rangle \equiv |j^{(1)}\rangle$. If these new bases define a closer classical state according to (46), then this step is accepted, and otherwise rejected. The latter enables us to avoid being trapped by a local minimum. This procedure is repeated until (a) a desired accuracy or (b) a predefined number of steps is reached. To compensate for the stochastic nature of Algorithm 1, ten initial local bases sets are chosen and the closest resulting classical state is taken as the optimal one. The step size parameter M is chosen to be 10^3, and the number of steps $N_{\text{step}} = 10^4$.

5. Numerical results

In this section, we present the main results of this paper, namely the correlation and entanglement pattern in the π-bonds of the molecular electronic ground states of π-conjugated organic molecules.

5.1. Ethylene

We first study one of the simplest molecules containing a prototypical π-bond, namely ethylene (C_2H_4). Since the π-bond comprises only two carbon centers, the resulting CAS contains only $n_e = n_o = 2$ or for short CAS(2,2), that is the bonding and anti-bonding orbitals π and π^*, which are constructive and destructive superposition of two p_z-orbitals (assuming bonding along the z-axis) on the two carbon atoms, respectively. For non-interacting electrons, both electrons would occupy the energetically more favorable π-orbital, forming a product state with respect to partitioning of the bonding and antibonding orbitals, as in (33), whereas electron interaction lifts the occupancy of the π^*-orbital to around 0.03 electron pair, thus introducing a small deviation from the aforementioned product state. From this simple observation, we should expect a low correlation and entanglement between the π- and π^*-orbital, and this is indeed what we conclude from our analysis in figure 3 for the common, *canonical* case. However, more correlation and entanglement will be recovered as we *fully* localize these two orbitals.

In figure 3 we listed the total correlation I, classical correlation C, quantum correlation Q, and entanglement E between the two orbitals based on canonical, PM-localized, and atomic-like orbitals. In addition, for each correlation quantity, the effect of P-SSR and N-SSR are taken into account in our analysis. Since the active space comprises in all three cases only two orbitals, it follows that single orbital correlation

C_2H_4					
Canonical	I	C	Q	E	
No SSR	0.2819	0.1410	0.1410	0.1410	
P-SSR	0.2819	0.1410	0.1410	0.1410	
N-SSR	0.1410	0.1410	0.0000	0.0000	
PM-localized	I	C	Q	E	
No SSR	0.2819	0.1410	0.1410	0.1410	
P-SSR	0.2819	0.1410	0.1410	0.1410	
N-SSR	0.1410	0.1410	0.0000	0.0000	
Atomic-like	I	C	Q	E	
No SSR	2.6468	1.3234	1.3234	1.3234	
P-SSR	2.0165	1.3234	0.6931	0.6931	
N-SSR	1.7916	1.3234	0.4682	0.4682	

Figure 3. Total correlation I, classical correlation C, quantum correlation Q, and entanglement E between two canonical, PM-localized, and atomic-like orbitals used for constructing the ground state of C_2H_4, for the case without SSR, with P-SSR, and with N-SSR. For each choice of orbital pair, contour plots (with an isosurface value of 0.05) of the orbitals are shown on the right most column.

and entanglement (those between one orbital and the rest of the system) will coincide with the orbital–orbital ones.

Starting with the canonical case (upper panel of figure 3), all correlation quantities are low, as anticipated above. In the case without SSRs and recalling that in this particular example the two-orbital reduced state is pure, the total correlation I is simply twice the amount of the classical C and quantum parts Q such that there is no distinction between quantum correlation Q and entanglement E. Interestingly, P-SSR does not show any diminishing effect in any of the correlation quantities. We can explain this somewhat surprising fact with the observation that the electronic ground state does not contain contributions from singly-excited configurations, and thus can solely be written as a superposition of doubly-occupied and empty configurations, respectively. Moreover, this is also the reason why no quantum correlation or entanglement survive in the presence of N-SSR: the ground state contains only a superposition of configurations with different local particle numbers.

Hence, in order to recover strong correlation and entanglement in the π-bond, we applied two different localization schemes to the canonical orbitals as detailed in section 4.1. In this particular case, the PM-localization scheme yields *localized* π-MOs matching the original canonical π-orbitals, since the system comprises only σ- and π-type orbitals and the PM-localization scheme preserves the σ- and π-character of the MOs. As a result, we see no difference in their respective correlation quantities with respect to the canonical case and the data for the PM case coincide in all three rows (see second panel in figure 3) with their respective counterpart in the upper panel of the canonical case. In passing we note that these findings will not hold when the canonical MOs span over several bonding regions, as we shall see in the following sections. Our second localization scheme sets out from the PM-localized MOs (in this case equivalently the canonical MOs) where we apply in an ensuing step a 2×2 Jacobi rotation between the two PM-localized orbitals by an angle $\theta = \frac{\pi}{4}$. This unitary rotation leads to two atomic-like orbitals

$$\psi_L = \frac{1}{\sqrt{2}}\pi_{\mathrm{PM}} + \frac{1}{\sqrt{2}}\pi^*_{\mathrm{PM}}, \tag{47a}$$

$$\psi_R = \frac{1}{\sqrt{2}}\pi_{\mathrm{PM}} - \frac{1}{\sqrt{2}}\pi^*_{\mathrm{PM}}, \tag{47b}$$

where $\pi^{(*)}_{\mathrm{PM}}$ are the PM-localized $\pi^{(*)}$-orbitals. As illustrated in the third panel of figure 3 (atomic-like), the resulting $\psi_{1,2}$ are indeed *fully localized* around one carbon center in stark contrast to the localized MOs obtained from the PM localization scheme. Moreover, these atomic-like orthogonal orbitals act *identically* as the original atomic orbitals, in a sense that the same linear combination of the former as the latter give rise to the bonding and antibonding orbitals (up to overall normalization)

$$\pi_{PM} = \frac{1}{\sqrt{2}}\psi_L + \frac{1}{\sqrt{2}}\psi_R,$$
$$\pi^*_{PM} = \frac{1}{\sqrt{2}}\psi_L - \frac{1}{\sqrt{2}}\psi_R, \tag{48}$$

thus preserving the information of the bond construction. And most importantly, we now recover strong correlation and entanglement in the π-bond. Without SSRs, the entanglement E between ψ_1 and ψ_2 reaches 95% of its maximum value of $2\ln 2$, in excellent agreement with the degree of entanglement that we observed for a prototypical bond in the analytic example discussed in section 3.2. Moreover, the effect of SSRs is qualitatively different in case of the atomic-like orbitals. P-SSR cancels around half of the entanglement, whereas around a third of the entanglement is still accessible under the restriction of N-SSR. The latter is rooted in the complexity of the ground state wave function which, in contrast to the much simpler form within the canonical and PM-localized orbitals bases, is now composed of several configurations of comparable weights, including those with single local occupations.

It is worth noting that the fully localized orbitals are only 95% maximally entangled. This deviation from the perfect single bond in section 3.2 is not an artefact of an imperfect choice of orbitals, but rather an inevitable consequence of electron interaction. The latter namely introduces a multireference character to the ground state, and excites finite occupation in the antibonding orbital. In other words, the maximal entanglement $2\ln 2$ in a perfect single bond state $f^\dagger_{\phi\uparrow} f^\dagger_{\phi\downarrow}|0\rangle$ can never be realized in an interacting molecule.

To summarize the main conclusions from this seemingly simple example, enforcing *atomic-like* locality in the MO basis for the π-orbital space leads to two distinct features of the π-bond in comparison to the commonly considered canonical case: (a) the ground state electronic wave function markedly changes character from single- to strongly multi-configurational and, more importantly, (b) the actual entanglement E between the valence $\pi^{(*)}$-orbitals without SSR increases drastically from 5% to 95% of its maximum value of $2\ln 2$ which was established by means of an analytical model for a chemical bond in section 3.2.

5.2. Polyene

Having analyzed in the previous section the conceptually most simple 'mono'-ene, we will focus in the following on all-*trans* polyenes CH_2–$(CH)_n$–CH_2, a family of extended, prototypical, π-conjugated molecular systems. More specifically, we consider two exemplary systems with $n = 8$ (decapentaene, $C_{10}H_{12}$) and $n = 18$ (eicosadecaene, $C_{20}H_{22}$). To unambiguously study the individual correlation contributions within the valence $\pi^{(*)}$-space requires for those molecular systems active orbital spaces of CAS(10,10) and CAS(20,20), respectively. Given the size of these CAS spaces, single-orbital and orbital–orbital correlations will no longer coincide, and need to be addressed separately. With $n_o > 2$, the single orbital correlation quantifies the correlation between one orbital and all other orbitals, including multipartite correlations, much beyond any orbital–orbital correlations. As in the case of ethylene in the previous section, we will consider for our analysis three distinct choices of MO basis, namely canonical, PM-localized, and atomic-like orbitals.

5.2.1. Single orbital correlation

As we are dealing with a pure ground state, single orbital correlation can be related to the single orbital entanglement via simple linear relations [68], and the latter is equivalent with the single-orbital quantum correlation. To this end, it suffices to focus in this paragraph solely on single-orbital entanglement data.

In figures 4 and 5, respectively, we present the canonical, PM-localized, and atomic-like orbitals for $C_{10}H_{12}$ and $C_{20}H_{22}$ (upper panels) along with the single orbital entanglement of each orbital (lower panels of figures 4 and 5), namely the entanglement between one orbital and the remaining orbitals comprised in the active space. Before embarking on an in-depth discussion of the entanglement data, we first emphasize two obvious key differences between the MOs of the polyenes shown in the upper panels of figures 4 and 5, respectively, and those of ethylene: (a) the canonical MOs for both extended systems are highly delocalized across the entire carbon–carbon chain; (b) the PM-localized MOs no longer coincide with the canonical ones, and are localized only around two carbon centers involved in a $\pi^{(*)}$-bond. Hence, the PM-localization scheme succeeds in *partially* localizing the canonical MOs. Finally, as was the case for ethylene, to obtain atomic-like orbitals requires a further rotation of each corresponding pair of PM-localized $\pi^{(*)}$-MOs by $\theta = \frac{\pi}{4}$.

Considering next the single orbital entanglement shown in the lower panels of the respective figures 4 and 5, the three choices of MO basis reveal drastically different behaviors. For both molecules, the canonical MOs display a large variation in their single orbital entanglement. The most entangled orbital #6 (#11 in $C_{20}H_{22}$) corresponds to the LUMO in either case and contains almost three times the amount of the least

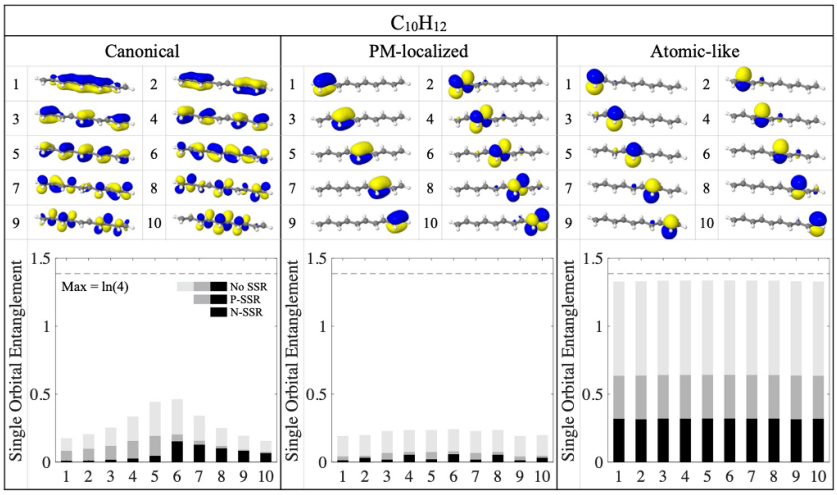

Figure 4. Single orbital entanglement in the CAS(10,10)-optimized electronic ground state of $C_{10}H_{12}$. The orbital numbering on the *x*-axis in the lower panel follows the one given for the canonical, PM-localized, and atomic-like orbitals in the upper panel (plotted with an isosurface value of 0.05). The color code for the single orbital entanglement data is as follows: no SSR (all color), P-SSR (black and dark grey), and N-SSR (dark grey).

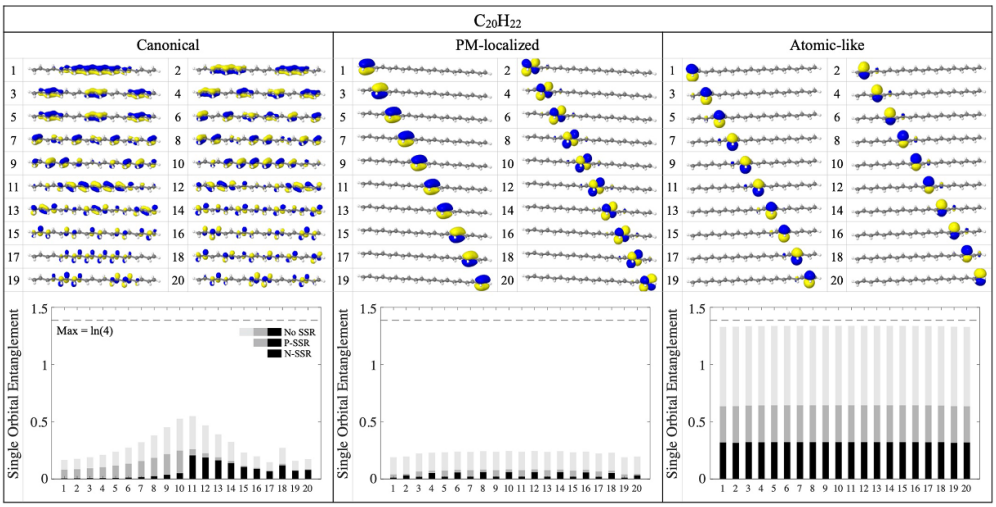

Figure 5. Single orbital entanglement in the CAS(20,20)-optimized electronic ground state of $C_{20}H_{22}$. The orbital numbering on the *x*-axis in the lower panel follows the one given for the canonical, PM-localized, and atomic-like orbitals in the upper panel (plotted with an isosurface value of 0.05). The color code for the single orbital entanglement data is as follows: no SSR (all color), P-SSR (black and dark grey), and N-SSR (dark grey).

entangled ones. The difference between the two SSRs manifests itself as follows: while the superselected entanglement (allowed by either P- or N-SSR) of the first half of the canonical π-MOs is mostly forbidden by N-SSR, that of the second half of the orbitals—corresponding to the π^*-manifold—is mostly N-SSR compatible. The fact that we still find single orbital entanglement for the π-orbitals is therefore a clear indication of their departure from a double occupancy (as would be expected in an uncorrelated mean-field model) in the CAS-optimized ground-state wave function due to the presence of electron–electron correlation which is most dominant for the HOMO and HOMO-1. Likewise, a similar explanation holds for P- and N-SSR single orbital entanglement data within the π^*-manifold where the discernible deviations between the two SSR schemes are a result of the departure from zero occupancy of the π^*-MOs, predominantly of the LUMO and LUMO + 1.

Naively, one would expect that the single orbital entanglement of the PM-localized and atomic-like orbitals should qualitatively show the same kind of deviation from that of the canonical MOs, with the latter being stronger for the atomic-like orbitals. However this is clearly not the case here. The single orbital entanglement of the PM-localized MOs is much more uniformly distributed than that of the canonical ones,

and overall visibly lower. On the one hand, the uniformity of the entanglement originates from the near translation invariance of the PM-localized MOs. Moreover, the entanglement differs only slightly from uniformity when the MO is located at the edge of the carbon–carbon chain, where a boundary effect comes into play. On the other hand, the lower value of entanglement of the PM-localized MOs is rooted in their geometrical shape. Each MO is centered around two carbon atoms involved in a chemical π-bond, effectively masking the entanglement of the bond within each MO itself. Interestingly, from the orbital plots shown in the upper panels of figures 4 and 5, we conclude that the PM-localized MOs can still be identified as either bonding π- or anti-bonding π^*-MOs. This classification remains also apparent in the superselected entanglement values. The bonding π-orbitals (with odd indices) contain mostly N-SSR forbidden entanglement whereas in the anti-bonding π^* ones (even indices) most superselected entanglement is N-SSR compatible, similar to the situation encountered within the canonical MO basis.

By contrast, the single orbital entanglement of the atomic-like orbitals is almost equally distributed. This finding is perhaps not surprising as the atomic-like orbitals are almost identical up to translation and a possible phase change. Furthermore, the closeness of agreement between the effects of applying either the P- or N-SSR for the single orbital entanglement is a clear indication that there are no favored orbitals among the manifold of $\pi^{(*)}$-MOs in terms of occupation numbers. In stark contrast to the PM-localized orbitals, the degree of entanglement becomes substantially higher than that of the canonical MOs, reaching 96% of the theoretical maximum of $2\ln 2$. To explain this finding, we recall that the atomic-like orbitals are, by construction, a superposition of bonding and anti-bonding PM-localized orbitals. Such a rotation between matching π–π^*-MOs entails a release of the entanglement tucked away within the PM-localized orbitals, and becomes manifest in an entanglement between the atomic-like orbitals . As we shall see in section 5.2.2, each atomic-like orbitals centered on one carbon atom has a pairwise entanglement with exactly only one other atomic-like orbital, localized around the second carbon center that is contributing to the same chemical bond.

5.2.2. Orbital–orbital correlations

In this section, we analyze the orbital–orbital correlations (classical, quantum, entanglement) in the ground states of $C_{10}H_{12}$ and $C_{20}H_{22}$, as a continuation of the previous section which focused on the single orbital entanglement. We consider the two-orbital reduced density states as the 'overall' state, which are typically mixed, and serve as our point of departure to study the correlation between any two orbitals (within our correlation model CAS space). In this scenario, the total correlation I is no longer linearly related to the entanglement E, and the latter is therefore always smaller or equal to the quantum correlation Q.

In order to enable an unambiguous comparison of correlation strengths throughout our various choices of MO bases, we define the following quantities as the pairwise total correlation sum I_{sum}, pairwise classical correlation sum C_{sum}, pairwise quantum correlation sum Q_{sum}, and pairwise entanglement sum E_{sum},

$$X_{\text{sum}}^{(\text{P, N})}(\{\phi_l\}, |\Psi\rangle) = \sum_{i<j} X\left(\rho_{ij}^{(\text{P, N})}\right) \qquad X = I, C, Q, E \tag{49}$$

where $\rho_{ij}^{(\text{P, N})}$ is the (P, N-SSR compatible) reduced state of $|\Psi\rangle$ on the orbital ϕ_i and ϕ_j of the specified basis set $\{\phi_l\}$.

In figures 6 and 7 we highlight the orbital–orbital total correlation I, classical correlation C, quantum correlation Q, and entanglement E between the canonical, PM-localized, and atomic-like orbitals in the ground states of $C_{10}H_{12}$ and $C_{20}H_{22}$, respectively. Moreover, the corresponding pairwise correlation sum is shown below each plot. We discuss in the following three major conclusions that can be drawn from the orbital–orbital correlation data.

We *first* observe a primarily low total correlation I between either canonical or PM-localized MOs, whereas the degree of correlation between the atomic-like orbitals is strikingly higher, exhibiting a six-fold increase in going from the PM-localized to the atomic-like orbitals basis. Simultaneously, the pairwise entanglement E reaches up to 91% of $2\ln 2$ for both $C_{10}H_{12}$ and $C_{20}H_{22}$. Moreover, in the atomic-like orbitals basis, we find that the pairwise quantum correlation Q can be as large as 94% of $2\ln 2$. We already saw in the case of C_2H_4 that 100% of maximal entanglement can never occur in an interacting molecule. Here however, the entanglement is further lowered due to the presence of orbital coupling. To see this we first notice that the two-orbital reduced states are now mixed, as a result of interaction between the two orbitals and the rest of the system. This degree of mixedness indicates that the two orbital system is also entangled with other orbitals, and hence naturally reduces the maximally achievable entanglement between them.

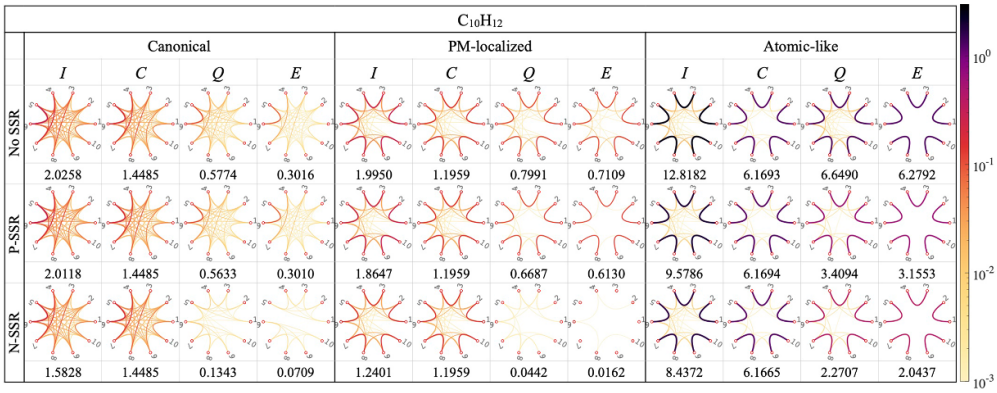

Figure 6. Pairwise orbital total correlation I, classical correlation C, quantum correlation Q, and entanglement E in the CAS(10,10)-optimized electronic ground state of $C_{10}H_{12}$ in case of no SSR, P-SSR, and N-SSR. The orbital numbering follows the one given for the canonical, PM-localized, and atomic-like orbitals in the upper panel of figure 4. The corresponding pairwise correlation sum (see equation (49)) is given below each plot.

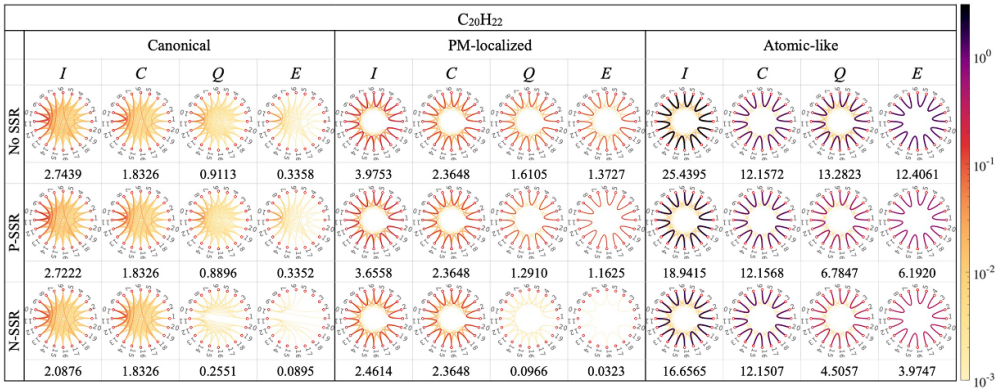

Figure 7. Pairwise orbital total correlation I, classical correlation C, quantum correlation Q, and entanglement E in the CAS(20,20)-optimized electronic ground state of $C_{20}H_{22}$ in case of no SSR, P-SSR, and N-SSR. The orbital numbering follows the one given for the canonical, PM-localized, and atomic-like orbitals in the upper panel of figure 5. The corresponding pairwise correlation sum (see equation (49)) is given below each plot.

In addition to a comparison of absolute correlation data, it is instructive to consider the relative contributions of quantum and classical correlation to the total correlation, focusing first on the case without SSRs. In the canonical MO basis, a larger portion of the total correlation is classical rather than quantum in nature. For example, the pairwise quantum correlation sum Q_{sum} in the ground state of $C_{10}H_{12}$ is only 29% of the pairwise total correlation sum I_{sum}, and, similarly, 33% for $C_{20}H_{22}$. As we move to the PM-localized MO basis, though the overall total correlation does not increase, the relative contribution of quantum correlation Q rises to 40% and 41% for $C_{10}H_{12}$ and $C_{20}H_{22}$ respectively. This effect becomes even more apparent in the atomic-like orbitals basis, where the fraction of quantum correlation (>52%) surpasses that of the classical correlation for both molecules. Furthermore, in passing from a canonical as well as PM-localized to an atomic-like orbitals basis, we not only observe an increase of the percentage of quantum correlation comprised in the total correlation, but also encounter a significant increase of the share of entanglement E in the quantum correlation. The latter increases from 37% and 85% to up to 93% for $C_{20}H_{22}$, as the orbitals are becoming more and more localized. *Secondly*, besides the effects on the importance of quantum correlation and entanglement, (almost fully) localizing the MOs introduces a distinct pairing structure. Among the canonical MOs, we do not find any obvious pairing structure except for those MOs located around the Fermi level (HOMO–LUMO, HOMO-1–LUMO-1) which also exhibit the largest pairwise correlations. Moving to the PM-localized MOs, a clear pairing structure emerges with pairs of MOs grouped together by relatively strong (total) pair-wise correlation and entanglement. Nonetheless, such a pair-wise correlation is still too weak to fully describe a chemical bond, compared to the maximal entanglement we found in section 3.2. The pattern observed in this case stems from the fact that the two

pairing MOs are the respective bonding π- and anti-bonding π^*-orbitals located primarily on the same two carbon atoms, an effect similar to the correlation between the canonical and PM-localized MOs in C_2H_4 in section 5.1. In a mean-field picture, all the local bonding orbitals are doubly occupied while the anti-bonding ones remain empty. By contrast, in a correlated picture electron–electron interaction introduces a finite occupation in the latter while simultaneously reducing the double-occupancy occupation of the former, thus creating a *weak* pair-wise correlation between the local bonding and anti-bonding orbitals. Considering next the atomic-like orbitals basis, the overall picture changes strikingly. The pronounced pairing structure of the correlation and entanglement data between MOs located on neighboring carbon atoms is an order of magnitude stronger than that of the PM-localized MOs. The pairwise entanglement E becomes even so strong that a so-called monogamy effect results, namely each atomic-like orbitals is *only* entangled to one other MO with which a bond is formed, in sharp contrast to the weak correlation background (yellow connecting lines) in the quantum correlation plots where MOs from different pairs are still correlated. This clear distinction indicates that (pair-wise) entanglement may be a more appropriate quantity to describe chemical bonds than quantum correlation would be.

Finally, we would like to highlight the effect of SSRs and their implication on the resulting complexity of the ground state wave function. For the canonical and PM-localized MO basis, P-SSR hardly changes the pairwise entanglement, whereas N-SSR suppresses almost all of it. This suggests that the dominating configurations in the total wave function are those with double or zero occupancy on the respective orbitals. In particular, the leading configurations are those where the bonding π-orbitals are doubly occupied rather than the anti-bonding π^* ones, giving rise to a weak pairing structure that could not survive in the presence of N-SSR. In other words, within the two-electron Hilbert space of two pairing orbitals (one bonding π_i and anti-bonding π_j^*), the leading configuration is simply $|\uparrow\downarrow\rangle_{\pi_i} \otimes |0\rangle_{\pi_j^*}$. Turning instead to atomic-like orbitals ϕ_i and ϕ_j that form a chemical bond, a far more complicated structure of the ground state emerges in this basis. For a given pair i,j of strongly entangled orbitals, none of the four configurations with fixed local occupation numbers

$$\begin{aligned} &|\uparrow\downarrow\rangle_{\phi_i} \otimes |0\rangle_{\phi_j}, \quad |0\rangle_{\phi_i} \otimes |\uparrow\downarrow\rangle_{\phi_j}, \\ &|\uparrow\rangle_{\phi_i} \otimes |\downarrow\rangle_{\phi_j}, \quad |\downarrow\rangle_{\phi_i} \otimes |\uparrow\rangle_{\phi_j}, \end{aligned} \tag{50}$$

in the two-electron Hilbert space is particularly dominating, as the entanglement is nearly at its maximum (if we only consider the two-electron subspace). This is also the reason why we encounter a strong P-SSR and N-SSR entanglement between the atomic-like orbitals . The drastically increased number of configurations with appreciable non-zero weight in the total wave function leads to a strongly, and *statically* correlated ground state description. Hence, even though an atomic-like orbitals basis is most suitable for a genuine description of a chemical bonding, in particular in terms of the pair-wise entanglement E, this basis, compared to the canonical and PM-localized counterparts, introduces a strong correlation structure in the electronic molecular ground state wave function. More importantly, though, the high degree of entanglement and quantum correlation even under P-SSR and N-SSR makes it a prime candidate in quantum computing applications.

To briefly summarize, we have successfully applied our orbital localization scheme first time to systems of realistic sizes, harnessing inspirations from both analytic example in section 3.2 and smaller concrete system, namely the ethylene molecule in section 5.1. Astonishingly, we were able to both locate and measure the intensity of the π-bonds using the monogamous entanglement between the fully-localized atomic-like orbitals, essentially breaking down the chain systems into units of ethylenes. The near maximal entanglement level we found in all the carbon chain systems established again that a single bond correspond to the entanglement value of $E = 2\ln 2$ between the two contributing atomic-like orbitals, though marginally lessened by electronic interaction. On one hand, our comprehensive QI framework offer surgical analysis of correlation and entanglement; on the other hand, the fully-localized atomic-like orbitals are the chemically meaningful subject of study. Together, they reveal a deep connection between bond order and the entanglement between the involved nuclear centers represented by the respective atomic-like orbitals, and offer a quantitative perspective to the valence bonding theory.

5.3. Benzene

Having discussed the linear, π-conjugated systems, we will in this section focus on the correlation pattern of the ground state of *the* prototypical, cyclic, π-conjugated aromatic molecule, namely benzene (C_6H_6).

To ease comparison, we perform the same correlation analysis as in section 5.2, by making use of the same three distinct sets of MO bases: canonical, PM-localized, and atomic-like orbitals , whose isosurfaces

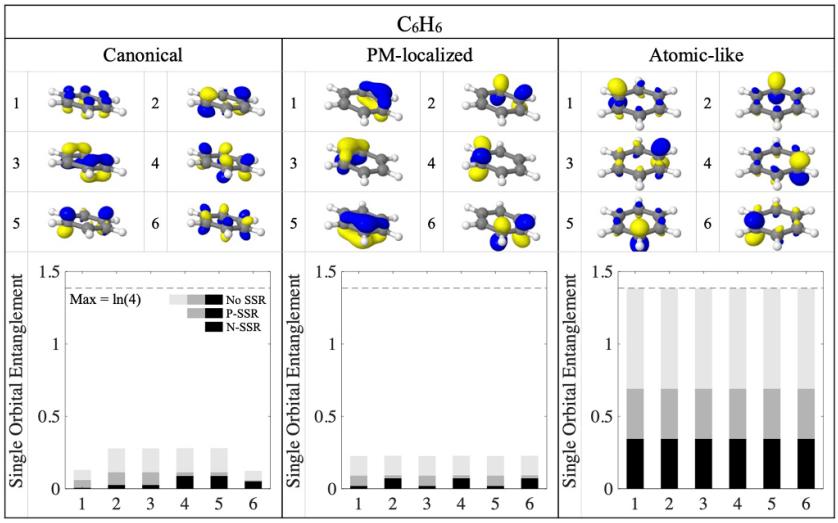

Figure 8. Single orbital entanglement in the CAS(6,6)-optimized electronic ground state of benzene. The orbital numbering on the x-axis in the lower panel follows the one given for the canonical, PM-localized, and atomic-like orbitals in the upper panel (plotted with an isosurface value of 0.05 for the canonical and PM-localized MOs, and 0.1 for the atomic-like orbitals). The color code for the single orbital entanglement data is as follows: no SSR (all color), P-SSR (black and dark grey), and N-SSR (dark grey).

are shown in figure 8. Before embarking on the correlation analysis, a comment is in order on how the atomic-like orbitals basis can be obtained for benzene. Compared to the other π-conjugated molecular systems, an atomic-like orbitals basis for benzene requires a generalized localization scheme. To explain this fact, we first point out that, for the polyenes, the PM-localized orbitals already indicated how atomic-like orbitals can be obtained. As we can see in figures 4 and 5, the PM-localized orbitals of $C_{10}H_{12}$ and $C_{20}H_{22}$ are of bonding and anti-bonding π-type, respectively, stretching primarily across two carbon centers. Making then use of the insight from our analytic example in section 3.2, it is straightforward to see that the respective atomic-like orbitals result from a unitary rotation with angle θ of the bonding and anti-bonding orbital pairs located on the same carbon centers by $\theta = \frac{\pi}{4}$. By contrast, such a pairing structure no longer emerges for the PM-localized basis in case of benzene. First, the PM-localized orbitals span over more than two carbon centers, due to the absence of a fixed local bonding region. Second, there is no obvious way of rotating any two orbitals which could give rise to atomic-like ones, solely based on geometrical considerations. Hence, we propose in the following a systematic way that leads to an atomic-like orbitals basis starting from the canonical rather than the PM-localized MO basis.

The canonical π-MOs of benzene (denoted as ϕ_i's) are linear combinations of atomic orbitals (LCAO)

$$\tilde{\phi}_i = \sum_j \mathbf{U}_{ij}\alpha_j. \tag{51}$$

where α_i's are the atomic orbitals and $\mathbf{U}$ a unitary matrix. Because the atomic orbitals have finite overlap with each other, the LCAO's need to be further normalized

$$\phi_i = \Lambda_{ij}\tilde{\phi}_j = (\Lambda\mathbf{U})_{ij}\alpha_j = \frac{\tilde{\phi}_i}{\|\tilde{\phi}_i\|}. \tag{52}$$

This last normalization transformation Λ makes the mapping $\Lambda\mathbf{U}$ from the atomic orbitals to the canonical orbitals non-unitary. Hence, we may ask ourselves what would happen if we transform the canonical orbitals by $\mathbf{U}^{-1}$? The resulting orbitals are still orthogonal of course, since $\mathbf{U}^{-1}$ is unitary. To assess the locality of these orbitals, we first consider an extreme example. Suppose that we have a molecule with internuclear distances such that all of its atomic orbitals (at different atomic centers) have vanishingly small overlap with each other. This entails that the LCAO's in equation (51) are already normalized ($\Lambda = \mathbb{1}$). Then the inverse transform

$$\tilde{\alpha}_i = \sum_j (\mathbf{U}^{-1})_{ij}\phi_j = \sum_j (\mathbf{U}^{-1}\Lambda\mathbf{U})_{ij}\alpha_j \tag{53}$$

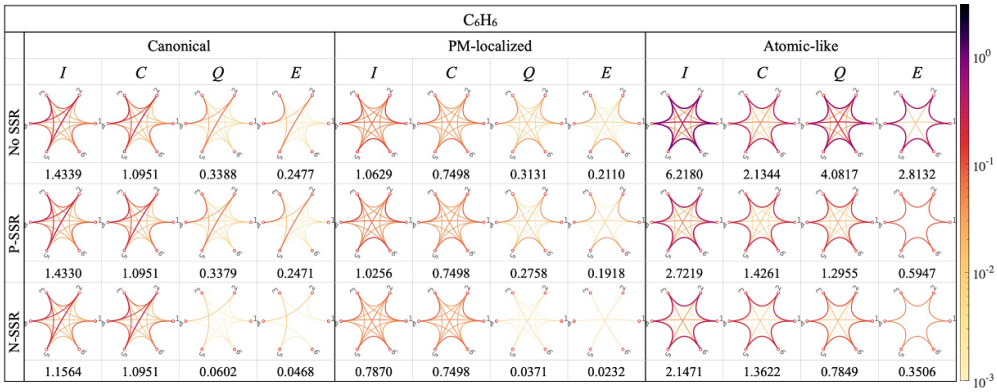

Figure 9. Pairwise orbital total correlation I, classical correlation C, quantum correlation Q, and entanglement E in the CAS(6,6)-optimized electronic ground state of benzene in case of no SSR, P-SSR, and N-SSR. The orbital numbering follows the one given for the canonical, PM-localized, and atomic-like orbitals in the upper panel of figure 8. The corresponding pairwise correlation sum (see equation (49)) is given below each plot.

would only give back the original atomic orbitals $\tilde{\alpha}_i = \sum_j (\mathbf{U}^{-1}\mathbf{U})_{ij}\alpha_j = \alpha_i$. When the atomic overlap is finite, Λ then deviates from the identity map, and so does $\mathbf{U}^{-1}\Lambda\mathbf{U}$. However, as long as the atomic overlap is not exceedingly large [90], Λ is close to an identity map, and each orbital $\overline{\alpha}_i$ will have a dominating contribution from the atomic orbital α_i and, simultaneously only small weights from the remaining ones, thus making the new *molecular* orbitals $\tilde{\alpha}_i$ atomic-like. Remarkably, our simple scheme does not refer to any cost function or require numerical optimization on a particular software platform. Furthermore, the atomic-like orbitals play the same role as the atomic orbitals in MO theory, in the sense that the same linear combinations of the atomic-like orbitals as those of the atomic ones reproduce the canonical MOs, up to a normalization factor.

Consequently, we applied for benzene the above localization scheme starting out from the canonical MO basis. As can be seen from figure 8, each atomic-like orbitals has a large contribution from a p_z-shaped *atomic* orbital on one carbon center, and only small weights from the remaining p_z-shaped orbitals on the other carbon centers. Moreover, all atomic-like orbitals are identical up to translations by an integer multiple of the lattice constant along the benzene ring. The localization scheme therefore successfully preserves the original shape of the atomic orbitals, while maintaining the orthogonality of the canonical ones.

In figures 8 and 9, respectively, we present the single-orbital and orbital–orbital correlation results for all three sets of MO bases. The correlation patterns within the canonical and PM-localized MO basis mainly resemble those of the linear polyenes discussed in the previous Subsection. In more detail, we first observe an overall low single orbital and orbital–orbital entanglement. Secondly, in the case without SSR most of the orbital–orbital correlation is again classical in nature with a share of 76% and 71%, respectively, of the orbital–orbital total correlation for the two MO bases. Thirdly, the distribution pattern of the superselected single orbital entanglement is also in alignment with previous findings. The bonding π-orbitals (odd indices in figure 8) have an occupancy close to the mean-field value of 2.0 and, consequently, only exhibit a small amount of N-SSR entanglement, whereas the occupancy in the anti-bonding π^*-MOs (even indices in figure 8) departs from its mean-field value of zero such that their superselected single orbital entanglement becomes N-SSR compatible.

Similar to the situation encountered for polyene systems, the correlation structure in the atomic-like orbitals basis becomes much richer. Considering first the single-orbital entanglement without SSR, we find that every atomic-like orbitals is maximally entangled (with value $2\ln 2$) with the rest of the system, as can be seen from figure 8. This strong entanglement is missing at the orbital–orbital level, though. A closer inspection of figure 9 reveals that the maximal pairwise entanglement E is considerably weaker than the one between the atomic-like orbitals in the polyenes. Compared to 92% of $2\ln 2$ for the latter, the maximum value of E in benzene amounts to merely 33% of $2\ln 2$. The origin of this discrepancy can be explained as follows. In sharp contrast to the pairing structure of the entanglement between the atomic-like orbitals in the polyenes, each atomic-like orbital on the benzene ring is equally entangled to *both* of its neighbors. This 'left-right pairing' is rooted in the underlying symmetry of the molecular Hamiltonian and closely resembles the simplified 'left-right overlap' model of the Hückel Hamiltonian for benzene [91]. Hence, the unique electronic ground state within our minimal π–π^* CAS(6,6) active orbital space enjoys the same symmetry as

the molecule itself, and is invariant under six-fold rotation and reflection about the mirror planes. A simplified, polyene-like pairing structure which would gives rise to a π-type bond involving only two neighboring carbon centers is therefore suppressed by the molecular symmetry. Although, even if we are to sum up the orbital–orbital entanglement between one orbital and both of its neighbors, 33% of the single orbital entanglement would not be accounted for from this partially summed *bipartite* orbital–orbital entanglement sum. As a result, we ascribe the missing part of the entanglement in this π-conjugated, aromatic molecule to genuine *multipartite* entanglement. Interestingly, for the cyclopropyl cation, the smallest 2-π-electron cyclic aromatic molecule (results not shown here), we do *not* encounter signs of entanglement beyond the orbital–orbital picture between the three carbon centers in the odd-numbered ring skeleton. Thus, whether multipartite entanglement is a distinct feature of π-conjugated, aromatic molecular systems with an *even* number of atomic centers contributing to the π-conjugation clearly deserves further investigation. While it goes beyond the scope of our current work, it will be subject of a future study.

6. Summary and conclusion

In this work we established a comprehensive QI framework for electronic structure analysis with the aim to foster synergies of the QI and QC communities within the second quantum revolution. This framework enabled us to dissect and compare quantum and classical effects in molecular systems, which closes an apparent gap in the current literature. This was made possible thanks to our unifying geometric picture of quantum states, which facilitated a unique definition of these correlation quantities on the same footing.

Under this framework, opened then up the possibility to quantify quantum correlation within molecules as a resource for information processing tasks. Still, since the amount of quantum correlation depends on the chosen orbital basis, we strove to maximize the resourcefulness of MOs through an orbital optimization scheme. The key idea of our scheme was to localize each MO to one atomic center only. This constituted a significant step beyond 'traditional' localization schemes (e.g. Pipek–Mezey (PM)) which typically yield final orbitals spanning over more than one nucleus. Combining both new essential ingredients—the comprehensive QI framework and our fully-localized orbitals—we arrived at two key results: (a) maximal resourcefulness of molecular systems is realized by fully-localized orbitals. (b) A single covalent bond is quantitatively best rationalized by the maximal orbital–orbital entanglement, that is $2\ln 2$.

To showcase these two crucial insights, we systematically compared various correlation quantities with respect to three important bases (canonical, PM-localized and fully-localized), in the ground states of π-conjugated chain systems (C_2H_4, $C_{10}H_{12}$ and $C_{20}H_{22}$). We observed almost maximal entanglement between the fully-localized orbitals, which is 9 and 37 times of the entanglement found in the PM-localized and canonical basis, respectively (comparing E_{sum} in $C_{20}H_{22}$). This drastic difference unequivocally shows that a fully-localized orbital basis is not only by far a superior reference but also reveals the abundant quantum resource inside these systems. Concomitantly, our analysis enabled us to associate *quantitatively* the existence of a chemical bond with the entanglement between fully-localized orbitals: each fully-localized orbital is only, *and* maximally, entangled with one other, together with which a bond is formed. Our entanglement analysis thus constitutes an important milestone in turning VB theory into a fully quantitative machinery.

To thoroughly further quantify the relation between chemical bonding and orbital entanglement, we also studied the prototypical aromatic molecule benzene. Unlike the polyene systems, the benzene ground state does not exhibit a conjugated π-bond structure. This is exactly reflected in our entanglement analysis: the entanglement in benzene is uniformly distributed, without an alternating pattern of strong and weak orbital–orbital entanglement. Yet, each fully-localized orbital was found to be maximally entangled with the complementary subsystem. The fact that this entanglement is not fully reflected in the orbital–orbital entanglement, confirms the commonly accepted picture that the π-bonds in benzene are shared within the entire ring rather than locally.

Finally, we would like to envisage a few promising directions sparked by the new framework we put forward in this work. Firstly, our quantitative rationalization of chemical bonding through entanglement analysis can be extended beyond π-bonds, such as to also encompass σ-type hybridized orbitals. The latter will therefore allow us to consider the vast majority of local bonds that dominate the chemical bonding of main group compounds. Secondly, we would like to strengthen the quantitative connection between orbital entanglement and highly delocalized, multicenter bonds, by exploring multipartite entanglement as a type of bonding descriptor, that is, for example, as an indicator for aromaticity. In conclusion, after showcasing versatile pathways to genuinely identify a potentially ample supply of quantum resource in chemical bonds, we look forward to spark an intense collaboration between the QI and QC communities in order to both harvest and further exploit these resources. This new prospect has the potential to bring about a paradigm-shifting change to modern chemistry: molecules are not only mere reactants in chemical processes

but also potent sources of entanglement and quantum correlations, the required resources for information processing tasks in the age of quantum technologies.

Data availability statement

The data that support the findings of this study are available upon reasonable request from the authors.

Acknowledgments

We thank S Mardazad for helpful discussions. We acknowledge financial support from the Deutsche Forschungsgemeinschaft (DFG, German Research Foundation), Grant SCHI 1476/1-1 (L D, C S), the Munich Center for Quantum Science and Technology (L D, C S) and the NKFIH through the Quantum Information National Laboratory of Hungary program, and Grants No. K124152, FK135220, K124351 (Z Z). The Project/research is also part of the Munich Quantum Valley, which is supported by the Bavarian state government with funds from the Hightech Agenda Bayern Plus.

Appendix A. Correlation sum rule

In this section we will show that the quantum and classical correlation of ρ sum up to the total correlation of ρ if its closest product state π_ρ and its closest classical state χ_ρ are simultaneously diagonalized.

We first observe that

$$I(\rho) - Q(\rho) - C(\rho) = S(\rho_A) + S(\rho_B) - S(\chi_A) - S(\chi_B), \tag{A1}$$

where $\chi_{A,B}$ are the reduced states of χ_ρ, respectively. We can then show that the spectrum of ρ_A and that of χ_A coincide. Let us denote the eigenstate of χ_ρ as $\{|i\rangle\otimes|j\rangle\}$. From this it follows that the eigenvalues of ρ_A are precisely its diagonal entries in this basis

$$\lambda_i = (\rho_A)_{ii} = \langle i|\rho_A|i\rangle = \sum_j \langle i|\otimes\langle j|\rho|i\rangle\otimes|j\rangle. \tag{A2}$$

Moreover, the eigenvalues of χ_A are given by

$$\begin{aligned}\mu_i &= \langle i|\mathrm{Tr}_B[\chi_\rho]|i\rangle \\ &= \langle i|\mathrm{Tr}_B\left[\sum_{kj}|k\rangle\langle k|\otimes|j\rangle\langle j|\rho|k\rangle\langle k|\otimes|j\rangle\langle j|\right]|i\rangle \\ &= \sum_j \langle i|\otimes\langle j|\rho|i\rangle\otimes|j\rangle = \lambda_i.\end{aligned} \tag{A3}$$

Using similar considerations, the spectrum of ρ_B and χ_B also coincide. As a result, the right-hand side of equation (A1) must vanish, leading to the sum rule

$$I(\rho) = Q(\rho) + C(\rho). \tag{A4}$$

This allows us to dissect the total correlation exactly into quantum and classical correlation contributions. When $\rho_{A,B}$ is not simultaneously diagonalized as $\chi_{A,B}$, its diagonal entries still coincide with those of $\chi_{A,B}$, namely the elements of $\vec{\mu}$. From this, it follows that the spectrum of $\rho_{A,B}$ given by $\vec{\lambda}$, majorizes $\vec{\mu}$, leading to the inequality $S(\rho_{A,B}) > S(\chi_{A,B})$. Hence, a general relation between the total, quantum, and classical correlation reads as

$$I(\rho) \geqslant Q(\rho) + C(\rho). \tag{A5}$$

Appendix B. Reference structures

Table B1. *XYZ* coordinates (in Å) of the benzene structure as taken from [92].

C	0.000 000 0000	1.396 792 0000	0.000 000 0000
C	0.000 000 0000	−1.396 792 0000	0.000 000 0000
C	1.209 657 0000	0.698 396 0000	0.000 000 0000
C	−1.209 657 0000	−0.698 396 0000	0.000 000 0000
C	−1.209 657 0000	0.698 396 0000	0.000 000 0000
C	1.209 657 0000	−0.698 396 0000	0.000 000 0000
H	0.000 000 0000	2.484 212 0000	0.000 000 0000
H	2.151 390 0000	1.242 106 0000	0.000 000 0000
H	−2.151 390 0000	−1.242 106 0000	0.000 000 0000
H	−2.151 390 0000	1.242 106 0000	0.000 000 0000
H	2.151 390 0000	−1.242 106 0000	0.000 000 0000
H	0.000 000 0000	−2.484 212 0000	0.000 000 0000

Table B2. *XYZ* coordinates (in Å) of the ethylene structure as taken from [93].

C	0.669 500 0000	0.000 000 0000	0.000 000 0000
C	−0.669 500 0000	0.000 000 0000	0.000 000 0000
H	1.232 100 0000	0.928 900 0000	0.000 000 0000
H	1.232 100 0000	−0.928 900 0000	0.000 000 0000
H	−1.232 100 0000	0.928 900 0000	0.000 000 0000
H	−1.232 100 0000	−0.928 900 0000	0.000 000 0000

Table B3. *XYZ* coordinates (in Å) of the decapentaene structure as taken from [94].

C	−5.570 819 0000	−0.217 743 0000	0.000 000 0000
H	−5.646 184 0000	−1.298 410 0000	0.000 000 0000
H	−6.495 732 0000	0.342 247 0000	0.000 000 0000
C	−4.373 490 0000	0.405 989 0000	0.000 000 0000
H	−4.347 960 0000	1.490 582 0000	0.000 000 0000
C	−3.085 856 0000	−0.277 393 0000	0.000 000 0000
H	−3.106 017 0000	−1.362 443 0000	0.000 000 0000
C	−1.885 150 0000	0.357 505 0000	0.000 000 0000
H	−1.868 794 0000	1.442 672 0000	0.000 000 0000
C	−0.600 421 0000	−0.318 770 0000	0.000 000 0000
H	−0.615 607 0000	−1.403 834 0000	0.000 000 0000
C	0.600 423 0000	0.318 772 0000	0.000 000 0000
H	0.615 610 0000	1.403 837 0000	0.000 000 0000
C	1.885 151 0000	−0.357 504 0000	0.000 000 0000
H	1.868 791 0000	−1.442 671 0000	0.000 000 0000
C	3.085 859 0000	0.277 388 0000	0.000 000 0000
H	3.106 026 0000	1.362 438 0000	0.000 000 0000
C	4.373 489 0000	−0.406 002 0000	0.000 000 0000
H	4.347 952 0000	−1.490 594 0000	0.000 000 0000
C	5.570 825 0000	0.217 717 0000	0.000 000 0000
H	5.646 212 0000	1.298 382 0000	0.000 000 0000
H	6.495 727 0000	−0.342 292 0000	0.000 000 0000

Table B4. *XYZ* coordinates (in Å) of the eicosadecaene structure as taken from [94].

C	−11.777 002 0000	−0.264 956 0000	0.000 000 0000
H	−11.838 826 0000	−1.346 690 0000	0.000 000 0000
H	−12.709 135 0000	0.283 328 0000	0.000 000 0000
C	−10.588 570 0000	0.373 284 0000	0.000 000 0000
H	−10.576 358 0000	1.458 319 0000	0.000 000 0000
C	−9.292 100 0000	−0.294 395 0000	0.000 000 0000
H	−9.299 259 0000	−1.379 813 0000	0.000 000 0000
C	−8.100 331 0000	0.354 687 0000	0.000 000 0000
H	−8.097 152 0000	1.440 196 0000	0.000 000 0000
C	−6.807 386 0000	−0.305 880 0000	0.000 000 0000
H	−6.809 239 0000	−1.391 233 0000	0.000 000 0000
C	−5.614 864 0000	0.346 177 0000	0.000 000 0000
H	−5.613 866 0000	1.431 609 0000	0.000 000 0000
C	−4.323 252 0000	−0.312 597 0000	0.000 000 0000
H	−4.324 092 0000	−1.397 991 0000	0.000 000 0000
C	−3.129 932 0000	0.339 737 0000	0.000 000 0000
H	−3.129 239 0000	1.425 156 0000	0.000 000 0000
C	−1.839 152 0000	−0.318 927 0000	0.000 000 0000
H	−1.840 033 0000	−1.404 337 0000	0.000 000 0000
C	−0.645 214 0000	0.333 028 0000	0.000 000 0000
H	−0.644 170 0000	1.418 440 0000	0.000 000 0000
C	0.645 057 0000	−0.326 167 0000	0.000 000 0000
H	0.643 670 0000	−1.411 588 0000	0.000 000 0000
C	1.839 395 0000	0.325 102 0000	0.000 000 0000
H	1.841 129 0000	1.410 508 0000	0.000 000 0000
C	3.129 491 0000	−0.334 960 0000	0.000 000 0000
H	3.127 312 0000	−1.420 391 0000	0.000 000 0000
C	4.323 931 0000	0.315 421 0000	0.000 000 0000
H	4.326 693 0000	1.400 812 0000	0.000 000 0000
C	5.614 248 0000	−0.345 956 0000	0.000 000 0000
H	5.610 823 0000	−1.431 395 0000	0.000 000 0000
C	6.808 433 0000	0.303 145 0000	0.000 000 0000
H	6.813 047 0000	1.388 490 0000	0.000 000 0000
C	8.099 575 0000	−0.360 992 0000	0.000 000 0000
H	8.093 201 0000	−1.446 493 0000	0.000 000 0000
C	9.293 393 0000	0.284 374 0000	0.000 000 0000
H	9.303 945 0000	1.369 761 0000	0.000 000 0000
C	10.587 573 0000	−0.387 745 0000	0.000 000 0000
H	10.571 407 0000	−1.472 733 0000	0.000 000 0000
C	11.778 381 0000	0.246 012 0000	0.000 000 0000
H	11.844 528 0000	1.327 487 0000	0.000 000 0000
H	12.708 325 0000	−0.305 984 0000	0.000 000 0000

Appendix C. Atomic-like orbitals in benzene

The pre-normalized canonical Hartree–Fock orbitals $\tilde{\phi}_i$'s of the benzene ring are related to the p_z orbitals α_i's by

$$\tilde{\phi}_i = \mathbf{U}_{ij}\alpha_j, \tag{C1}$$

where

$$\mathbf{U} = \begin{pmatrix} \frac{1}{\sqrt{6}} & \frac{1}{\sqrt{6}} & \frac{1}{\sqrt{6}} & \frac{1}{\sqrt{6}} & \frac{1}{\sqrt{6}} & \frac{1}{\sqrt{6}} \\ -\frac{1}{\sqrt{12}} & -\frac{1}{\sqrt{3}} & -\frac{1}{\sqrt{12}} & \frac{1}{\sqrt{12}} & \frac{1}{\sqrt{3}} & \frac{1}{\sqrt{12}} \\ \frac{1}{2} & 0 & -\frac{1}{2} & -\frac{1}{2} & 0 & \frac{1}{2} \\ -\frac{1}{2} & 0 & \frac{1}{2} & -\frac{1}{2} & 0 & \frac{1}{2} \\ -\frac{1}{\sqrt{12}} & \frac{1}{\sqrt{3}} & -\frac{1}{\sqrt{12}} & -\frac{1}{\sqrt{12}} & \frac{1}{\sqrt{3}} & -\frac{1}{\sqrt{12}} \\ \frac{1}{\sqrt{6}} & -\frac{1}{\sqrt{6}} & \frac{1}{\sqrt{6}} & -\frac{1}{\sqrt{6}} & \frac{1}{\sqrt{6}} & -\frac{1}{\sqrt{6}} \end{pmatrix}. \tag{C2}$$

The atomic-like orbitals $\tilde{\alpha}_i$ proposed by us is then obtained by applying the inverse $\mathbf{U}^{-1}$ to the *normalized* canonical Hartree–Fock orbitals $\phi_i = \tilde{\phi}_i/\|\tilde{\phi}_i\|$

$$\tilde{\alpha}_i = \mathbf{U}^{-1}_{ij}\phi_j. \tag{C3}$$

The above transformation can be achieved by a sequence of two-orbital rotations.

- **Step 1**

$$\begin{aligned}
\phi_1 &\leftarrow -\frac{1}{\sqrt{2}}\phi_1 + \frac{1}{\sqrt{2}}\phi_6, \quad & \phi_1 &\leftarrow \frac{1}{\sqrt{2}}\phi_1 + \frac{1}{\sqrt{2}}\phi_6 \\
\phi_2 &\leftarrow -\frac{1}{\sqrt{2}}\phi_2 + \frac{1}{\sqrt{2}}\phi_5, \quad & \phi_5 &\leftarrow \frac{1}{\sqrt{2}}\phi_2 + \frac{1}{\sqrt{2}}\phi_5 \\
\phi_3 &\leftarrow -\frac{1}{\sqrt{2}}\phi_3 + \frac{1}{\sqrt{2}}\phi_4, \quad & \phi_4 &\leftarrow \frac{1}{\sqrt{2}}\phi_3 + \frac{1}{\sqrt{2}}\phi_4
\end{aligned}$$

- **Step 2**

$$\begin{aligned}
\tilde{\alpha}_1 &\leftarrow -\frac{1}{\sqrt{3}}\phi_1 + \sqrt{\frac{2}{3}}\phi_2, \quad & \phi_2 &\leftarrow \sqrt{\frac{2}{3}}\phi_1 + \frac{1}{\sqrt{3}}\phi_2 \\
\phi_5 &\leftarrow -\frac{1}{\sqrt{3}}\phi_5 + \sqrt{\frac{2}{3}}\phi_6, \quad & \tilde{\alpha}_6 &\leftarrow \sqrt{\frac{2}{3}}\phi_5 + \frac{1}{\sqrt{3}}\phi_6
\end{aligned}$$

- **Step 3**

$$\begin{aligned}
\tilde{\alpha}_2 &\leftarrow -\frac{1}{\sqrt{2}}\phi_2 - \frac{1}{\sqrt{2}}\phi_4, \quad & \tilde{\alpha}_4 &\leftarrow -\frac{1}{\sqrt{2}}\phi_2 + \frac{1}{\sqrt{2}}\phi_4 \\
\tilde{\alpha}_3 &\leftarrow -\frac{1}{\sqrt{2}}\phi_3 + \frac{1}{\sqrt{2}}\phi_5, \quad & \tilde{\alpha}_5 &\leftarrow \frac{1}{\sqrt{2}}\phi_3 + \frac{1}{\sqrt{2}}\phi_5
\end{aligned}$$

We then arrive at the atomic-like orbitals $\tilde{\alpha}_i$'s.

ORCID iD

Christian Schilling https://orcid.org/0000-0001-6781-4111

References

[1] Dowling J P and Milburn G J 2003 Quantum technology: the second quantum revolution *Phil. Trans. R. Soc.* A **361** 1655–74
[2] Atzori M and Sessoli R 2019 The second quantum revolution: role and challenges of molecular chemistry *J. Am. Chem. Soc.* **141** 11339–52
[3] Deutsch I H 2020 Harnessing the power of the second quantum revolution *PRX Quantum* **1** 020101
[4] Friis N, Lee A R and Bruschi D E 2013 Fermionic-mode entanglement in quantum information *Phys. Rev.* A **87** 022338
[5] Friis N 2016 Reasonable fermionic quantum information theories require relativity *New J. Phys.* **18** 033014
[6] Gigena N and Rossignoli R 2015 Entanglement in fermion systems *Phys. Rev.* A **92** 042326
[7] Franco R L and Compagno G 2018 Indistinguishability of elementary systems as a resource for quantum information processing *Phys. Rev. Lett.* **120** 240403
[8] Ding L and Schilling C 2020 Correlation paradox of the dissociation limit: a quantum information perspective *J. Chem. Theory Comput.* **16** 4159–75
[9] Morris B, Yadin B, Fadel M, Zibold T, Treutlein P and Adesso G 2020 Entanglement between identical particles is a useful and consistent resource *Phys. Rev.* X **10** 041012
[10] Aoto Y A and da Silva M F 2020 Calculating the distance from an electronic wave function to the manifold of slater determinants through the geometry of Grassmannians *Phys. Rev.* A **102** 052803
[11] Olofsson E, Samuelsson P, Brunner N and Potts P P 2020 Quantum teleportation of single-electron states *Phys. Rev.* B **101** 195403
[12] Galler A and Thunström P 2021 Orbital and electronic entanglement in quantum teleportation schemes *Phys. Rev. Res.* **3** 033120
[13] Faba J, Martín V and Robledo L 2021 Correlation energy and quantum correlations in a solvable model *Phys. Rev.* A **104** 032428
[14] Faba J, Martín V and Robledo L 2021 Two-orbital quantum discord in fermion systems *Phys. Rev.* A **103** 032426
[15] Faba J, Martín V and Robledo L 2022 Analysis of quantum correlations within the ground state of a three level Lipkin model (arXiv:2203.09400)
[16] Benatti F, Floreanini R, Franchini F and Marzolino U 2020 Entanglement in indistinguishable particle systems *Phys. Rep.* **878** 1–27
[17] Sperling J and Agudelo E 2022 Entanglement of particles versus entanglement of fields: independent quantum resources (arXiv:2204.06245)
[18] Boguslawski K, Tecmer P, Legeza O and Reiher M 2012 Entanglement measures for single-and multireference correlation effects *J. Phys. Chem. Lett* **3** 3129–35
[19] Boguslawski K, Tecmer P, Barcza G, Legeza O and Reiher M 2013 Orbital entanglement in bond-formation processes *J. Chem. Theory Comput.* **9** 2959–73

[20] Mottet M, Tecmer P, Boguslawski K, Legeza O and Reiher M 2014 Quantum entanglement in carbon–carbon, carbon–phosphorus and silicon–silicon bonds *Phys. Chem. Chem. Phys.* **16** 8872–80
[21] Freitag L, Knecht S, Keller S F, Delcey M G, Aquilante F, Bondo Pedersen T, Lindh R, Reiher M and González L 2015 Orbital entanglement and CASSCF analysis of the Ru–NO bond in a ruthenium nitrosyl complex *Phys. Chem. Chem. Phys.* **17** 14383–92
[22] Duperrouzel C, Tecmer P, Boguslawski K, Barcza G, Legeza O and Ayers P W 2015 A quantum informational approach for dissecting chemical reactions *Chem. Phys. Lett.* **621** 160–4
[23] Zhao Y, Boguslawski K, Tecmer P, Duperrouzel C, Barcza G, Legeza O and Ayers P W 2015 Dissecting the bond-formation process of d^{10}-metal-ethene complexes with multireference approaches *Theor. Chem. Acc.* **134** 120
[24] Boguslawski K and Tecmer P 2015 Orbital entanglement in quantum chemistry *Int. J. Quantum Chem.* **115** 1289
[25] Szalay S, Barcza G, Szilvási T, Veis L and Legeza O 2017 The correlation theory of the chemical bond *Sci. Rep* **7** 1–10
[26] Stein C J and Reiher M 2017 Measuring multi-configurational character by orbital entanglement *Mol. Phys.* **115** 2110–9
[27] Stemmle C, Paulus B and Legeza O 2018 Analysis of electron-correlation effects in strongly correlated systems (N_2 and N_2^+) by applying the density-matrix renormalization-group method and quantum information theory *Phys. Rev.* A **97** 022505
[28] Brandejs J, Veis L, Szalay S, Barcza G, Pittner J and Legeza O 2019 Quantum information-based analysis of electron-deficient bonds *J. Chem. Phys* **150** 204117
[29] Pusuluk O, Yesiller M H, Torun G, Müstecaplıoğlu O E, Yurtsever E and Vedral V 2021 Classical and quantum orbital correlations in the molecular electronic states (arXiv:2107.13992)
[30] Krumnow C, Veis L, Legeza O and Eisert J 2016 Fermionic orbital optimization in tensor network states *Phys. Rev. Lett.* **117** 210402
[31] Stein C J and Reiher M 2016 Automated selection of active orbital spaces *J. Chem. Theory Comput.* **12** 1760
[32] Turner C J, Meichanetzidis K, Papić Z and Pachos J K 2017 Optimal free descriptions of many-body theories *Nat. Commun.* **8** 1–7
[33] Wick G-C, Wightman A S and Wigner E P 1970 Superselection rule for charge *Phys. Rev.* D **1** 3267
[34] Wick G-C, Wightman A S and Wigner E P 1997 The intrinsic parity of elementary particles *Part I: Particles and Fields. Part II: Foundations of Quantum Mechanics* (Berlin: Springer) p 102
[35] Ollivier H and Zurek W H 2001 Quantum discord: a measure of the quantumness of correlations *Phys. Rev. Lett.* **88** 017901
[36] Luo S and Fu S 2010 Geometric measure of quantum discord *Phys. Rev.* A **82** 034302
[37] Henderson L and Vedral V 2001 Classical, quantum and total correlations *J. Phys. A: Math. Gen.* **34** 6899
[38] Vedral V, Plenio M B, Rippin M A and Knight P L 1997 Quantifying entanglement *Phys. Rev. Lett.* **78** 2275
[39] Wootters W K 1998 Entanglement of formation of an arbitrary state of two qubits *Phys. Rev. Lett.* **80** 2245
[40] Horodecki R, Horodecki P, Horodecki M and Horodecki K 2009 Quantum entanglement *Rev. Mod. Phys.* **81** 865
[41] Muller P 1994 Glossary of terms used in physical organic chemistry (IUPAC Recommendations 1994) *Pure Appl. Chem.* **66** 1090
[42] Roos B, Borin A C and Gagliardi L 2007 Reaching the maximum multiplicity of the covalent chemical bond *Angew. Chem., Int. Ed.* **46** 1469–72
[43] Shaik S and Hiberty P C 2004 *Valence Bond Theory, Its History, Fundamentals and Applications: A Primer* (New York: Wiley) ch 1, pp 1–100
[44] Goddard W A III, Dunning T H Jr, Hunt W J and Hay P J 1973 Generalized valence bond description of bonding in low-lying states of molecules *Acc. Chem. Res.* **6** 368–76
[45] In a strict mathematical sense the quantum relative entropy does not define a distance function. For instance, it is not symmetric, i.e. $S(\rho||\pi) \neq S(\pi||\rho)$ and it does in general not obey the triangle inequality
[46] Lindblad G 1974 Expectations and entropy inequalities for finite quantum systems *Commun. Math. Phys.* **39** 111–9
[47] Vedral V 2002 The role of relative entropy in quantum information theory *Rev. Mod. Phys.* **74** 197
[48] Hiai F and Petz D 1991 The proper formula for relative entropy and its asymptotics in quantum probability *Commun. Math. Phys.* **143** 99
[49] Werner R F 1989 Quantum states with Einstein–Podolsky–Rosen correlations admitting a hidden-variable model *Phys. Rev.* A **40** 4277
[50] Nielsen M A and Chuang I 2002 Quantum computation and quantum information *Am. J. Phys.* **70** 558
[51] Modi K, Paterek T, Son W, Vedral V and Williamson M 2010 Unified view of quantum and classical correlations *Phys. Rev. Lett.* **104** 080501
[52] Wolf M M, Verstraete F, Hastings M B and Cirac J I 2008 Area laws in quantum systems: mutual information and correlations *Phys. Rev. Lett.* **100** 070502
[53] Watrous J 2011 Lecture notes on the "theory of quantum information (available at: https://cs.uwaterloo.ca/~watrous/TQI-notes/)
[54] Schilling C 2021 Orbital entanglement and correlation *Simulating Correlations With Computers* ed E Pavarini and E Koch (Verlag: Forschungszentrum Jülich GmbH Zentralbibliothek) ch 9, p 261
[55] Henderson L and Vedral V 2000 Information, relative entropy of entanglement and irreversibility *Phys. Rev. Lett.* **84** 2263–6
[56] Ding L, Zimboras Z and Schilling C 2022 Quantifying electron entanglement faithfully (arXiv:2207.03377)
[57] Ekert A and Knight P L 1995 Entangled quantum systems and the schmidt decomposition *Am. J. Phys.* **63** 415–23
[58] Eisert J, Cramer M and Plenio M B 2010 Colloquium: Area laws for the entanglement entropy *Rev. Mod. Phys.* **82** 277
[59] Kitaev A and Preskill J 2006 Topological entanglement entropy *Phys. Rev. Lett.* **96** 110404
[60] Laflorencie N 2016 Quantum entanglement in condensed matter systems *Phys. Rep.* **646** 1–59
[61] Wootters W K 1998 Quantum entanglement as a quantifiable resource *Phil. Trans. R. Soc. London, Ser.* A **356** 1717
[62] Bouwmeester D, Pan J-W, Mattle K, Eibl M, Weinfurter H and Zeilinger A 1997 Experimental quantum teleportation *Nature* **390** 575
[63] Ursin R *et al* 2007 Entanglement-based quantum communication over 144 km *Nat. Phys.* **3** 481–6
[64] Jennewein T, Simon C, Weihs G, Weinfurter H and Zeilinger A 2000 Quantum cryptography with entangled photons *Phys. Rev. Lett.* **84** 4729
[65] Oppenheim J, Horodecki M, Horodecki P and Horodecki R 2002 Thermodynamical approach to quantifying quantum correlations *Phys. Rev. Lett.* **89** 180402
[66] Luo S 2008 Using measurement-induced disturbance to characterize correlations as classical or quantum *Phys. Rev.* A **77** 022301
[67] Johansson M 2016 Comment on 'Reasonable fermionic quantum information theories require relativity' (arXiv:1610.00539)
[68] Ding L, Mardazad S, Das S, Szalay S, Schollwöck U, Zimborás Z and Schilling C 2020 Concept of orbital entanglement and correlation in quantum chemistry *J. Chem. Theory Comput.* **17** 79–95
[69] Wick G-C, Wightman A S and Wigner E P 1952 The intrinsic parity of elementary particles *Phys. Rev.* **88** 101
[70] Bartlett S D and Wiseman H M 2003 Entanglement constrained by superselection rules *Phys. Rev. Lett.* **91** 097903

[71] Verstraete F and Cirac J I 2003 Quantum nonlocality in the presence of superselection rules and data hiding protocols *Phys. Rev. Lett.* **91** 010404
[72] Krylov A I 2020 From orbitals to observables and back *J. Chem. Phys.* **153** 080901
[73] Amosov G G and Filippov S N 2017 Spectral properties of reduced fermionic density operators and parity superselection rule *Quantum Inf. Process.* **16** 1–16
[74] Atkins P W and Friedmann R S 1996 *Molecular Quantum Chemistry* (Oxford: Oxford University Press)
[75] White S R 1992 Density matrix formulation for quantum renormalization groups *Phys. Rev. Lett.* **69** 2863–6
[76] White S R 1993 Density-matrix algorithms for quantum renormalization groups *Phys. Rev.* B **48** 10345
[77] Schollwöck U 2011 The density-matrix renormalization group in the age of matrix product states *Ann. Phys.* **326** 96
[78] Baiardi A and Reiher M 2020 The density matrix renormalization group in chemistry and molecular physics: Recent developments and new challenges *J. Chem. Phys.* **152** 040903
[79] Werner H-J, Knowles P J, Knizia G, Manby F R and Schütz M 2012 *Wiley Interdiscip. Rev.-Comput. Mol. Sci.* **2** 242–53
[80] Werner H-J *et al* 2020 *J. Chem. Phys.* **152** 144107
[81] Werner H-J *et al* 2019 MOLPRO, version 2019, a package of *ab initio* programs (available at: www.molpro.net)
[82] Knowles P J and Handy N C 1989 A determinant based full configuration interaction program *Comput. Phys. Commun.* **54** 75–83
[83] Keller S, Dolfi M, Troyer M and Reiher M 2015 An efficient matrix product operator representation of the quantum-chemical Hamiltonian *J. Chem. Phys.* **143** 244118
[84] Keller S and Reiher M 2016 Spin-adapted matrix product states and operators *J. Chem. Phys.* **144** 134101
[85] Knecht S, Hedegaard E D, Keller S, Kovyrshin A, Ma Y, Muolo A, Stein C J and Reiher M 2016 New approaches for *ab initio* calculations of molecules with strong electron correlation *Chimia* **70** 244–51
[86] Dunning Jr T H 1989 Gaussian basis sets for use in correlated molecular calculations. I. The atoms boron through neon and hydrogen *J. Chem. Phys.* **90** 1007
[87] Pipek J and Mezey P G 1989 A fast intrinsic localization procedure applicable for *ab initio* and semiempirical linear combination of atomic orbital wave functions *J. Chem. Phys.* **90** 4916
[88] Koridon E, Yalouz S, Senjean B, Buda F, O'Brien T E and Visscher L 2021 Orbital transformations to reduce the 1-norm of the electronic structure Hamiltonian for quantum computing applications *Phys. Rev. Res.* **3** 033127
[89] 2021 Jmol: an open-source java viewer for chemical structures in 3D (available at: www.jmol.org)
[90] For example, straightforward calculation would show for the case of two identical atomic orbitals with overlap of 0.75, each resulting atomic-like orbital is still dominated by one atomic orbital with 69% relative weight
[91] Hückel E 1931 Quantentheoretische beiträge zum benzolproblem. I. Die elektronenkonfiguration des benzols und verwandter verbindungen *Z. Phys.* **70** 204–86
[92] Eriksen J J *et al* 2020 The ground state electronic energy of benzene *J. Phys. Chem. Lett.* **11** 8922–9
[93] Herzberg G 1966 *Electronic Spectra and Electronic Structure of Polyatomic Molecules* (New York: Van Nostrand)
[94] Hu W and Chan G K-L 2015 Excited-state geometry optimization with the density matrix renormalization group, as applied to polyenes *J. Chem. Theory Comput.* **11** 3000–9